

2005年 8月
碩士學位論文

Nano Step Profile Measurement and Laser
Stabilization by Using the Interferometer

朝鮮大學校大學院

光應用工學科

刘震

Nano Step Profile Measurement and Laser Stabilization by Using the Interferometer

간섭계를 이용한 나노 계단 형상 측정 및 레이저 안정화

2005年 8月

朝鮮大學校大學院

光應用工學科

刘震

Nano Step Profile Measurement and Laser
Stabilization by Using the Interferometer

指導教授 金 珍 泰

이 論文을 工學碩士學位申請 논문으로 提出함

2005年 8 月

朝 鮮 大 學 校 大 學 院

光 應 用 工 學 科

刘 震

刘震의 碩士學位論文을 認准함

委員長 朝鮮大學校 助教授 金 玆 秀 印

委 員 朝鮮大學校 助教授 金 珍 泰 印

委 員 朝鮮大學校 助教授 朴 鍾 洛 印

2005 年 8 月

朝鮮大學校 大學院

Abstract

Nano Step Profile Measurement and Laser Stabilization by Using the Interferometer

by Liu Zhen

Advisor: Professor Kim, Jin-Tae, Ph.D.

Department of Photonic Engineering

Graduate School of Chosun University

In this thesis, we introduced two experiments. One is height measurement of reference step with 93.1 nm thickness by using stabilized interferometer and FFT method, another one is laser stabilization and hyperfine structure measurement by using tilt locking method. The PID controller was employed in two experiments for stabilization system.

In order to measure the height measurement of reference, we developed a program in mathcad software. First we simulated FFT in 1D and 2D profile to check whether our generated mathcad codes are correct or not by using Tekeda and Kreis method. Before we did the simulation, we had introduced some basic knowledge about FFT and compared FFT with phase shift method. Then we used FFT method to measure the reference step height with thickness 93 nm in the highly

windy environmental conditions. After obtaining the value of the reference step height, we compared it with the measurement in vibrationless conditions with commercial Mirau type interferometer using Accura2000 system. Except above contents, we also introduced some basic knowledge and procedure of tuning the parameters of PID controller so as to get the stabilization of Twyman-Green interferometer. As the result, the reference step height with the thickness (93.1 ± 1.2 nm) has been measured.

In another case, we introduced how to stabilize the frequency of diode laser using tilt locking technique. First we introduced the historical background of tilt locking method and drew the comparison between it with other traditional methods. We set up a Sagnac interferometer to create an error due to phase shift. Phase shift is derived from the changing of refractive index of atom. In order to demonstrate the principle clearly, the first two Hermite-Gauss modes TEM_{00} and TEM_{01} are introduced. The hyperfine manifolds [$5^2S_{1/2}$ $F_3 \rightarrow F'=2, 3, 4$, $5^2P_{3/2}$ ^{85}Rb] is obtained using the error signal finally. The PID controller is employed in the experiment with the Sagnac interferometer together to make up of the servo loop and get the modulation-free frequency locking of a diode laser. As the result, the laser frequency is stabilized up to sub-megahertz level in the experiment.

Contents

| | |
|---|-----|
| Abstract | |
| Contents..... | I |
| List of figures..... | III |
| List of tables..... | VI |
| Introduction..... | 1 |
| I. Stabilization of surface measurement with Fast Fourier Transform method by PID controller..... | 4 |
| 1. The numerical simulation of surface profile measurement by Fast Fourier Transform method..... | 4 |
| 1.1 Introduction of Fast Fourier Transform method..... | 4 |
| 1.2 The simulation of the profile measurement in one-dimension..... | 16 |
| 1.3 The simulation of the profile measurement in two-dimensions..... | 33 |
| 2. The experiment and analysis of stabilization of surface profile(step height) measurement with FFT method by PID controller..... | 40 |
| 2.1 Introduction of PID controller..... | 40 |
| 2.2 Introduction of experiment..... | 45 |
| 2.3 The procedure of tuning the parameters of PID controller.... | 46 |
| 2.4 Discussion about the order of fringe stabilization..... | 48 |
| 2.5 Application of the PZT controller..... | 49 |
| 2.6 The results of the step height measurement with FFT method and roughness amplitude parameters | 52 |
| 2.7 Surface measurement by ACCURA system..... | 55 |

| | | |
|-------|--|----|
| 2.8 | The comparison of the results between with stabilization and without stabilization, and comparison of results between by FFT method and by ACCURA 2000 system..... | 57 |
| II. | The frequency stabilization of diode laser by PID controller.. | 59 |
| 3. | The frequency stabilization of diode laser with PID controller.. | 59 |
| 3.1 | Introduction and Principles..... | 59 |
| 3.1.1 | Introduction..... | 59 |
| 3.1.2 | Basic knowledge about characteristic of Rubidium..... | 60 |
| 3.2 | Experimental setup and analysis for the results of experiment..... | 61 |
| 3.2.1 | Tilt locking..... | 62 |
| 3.3 | The set up of the experiment..... | 65 |
| 3.4 | Results of the experiment and Discussion..... | 68 |
| | Acknowledgement..... | 73 |
| | References..... | 74 |
| | Appendix..... | 77 |

List of Figures

| | | |
|-----------------|--|-------|
| Fig.1.1 | The graph of inverse tangent function..... | 9 |
| Fig.1.2 | Unwrap the inverse tangent function from π modulo into 2π modulo..... | 10 |
| Fig.1.3 | (a): Wrapped phase, the range of value is restricted in π modulo. (b): Unwrapped phase by estimating the point of phase jump..... | 12 |
| Fig.1.4 | Unwrapping program flow chart in one dimension..... | 13 |
| Fig.1.5 | The concept of path dependent unwrapping algorithm in two dimensions..... | 14 |
| Fig.1.6 | Twyman-Green interferometry..... | 17 |
| Fig.1.7 | The graph of the surface profile function, the surface is tilted in a small angle..... | 19 |
| Fig.1.8 | The intensity function of interference pattern..... | 19 |
| Fig.1.9 | The amplitude distribution in the frequency domain after FFT..... | 20 |
| Fig.1.10 | The graph of the low frequency component..... | 21 |
| Fig.1.11 | The wrapped phase from $-\pi/2$ to $\pi/2$ | 22 |
| Fig.1.12 | The partial unwrapped phase only from $-\pi$ to π | 22 |
| Fig.1.13 | The partial unwrapped phase only from 0 to 2π | 23 |
| Fig.1.14 | Comparison between the original profile and the calculated profile..... | 24 |
| Fig.1.15 | (a): Plane surface (b): Interference for plane surface (c): Get the carrier frequency from frequency domain...25~26 | 25~26 |
| Fig.1.16 | $C(u-u_0)$ and $C^*(u+u_0)$ are centered around..... | 27 |
| Fig.1.17 | Function $C(u-u_0)$ | 28 |

| | |
|---|----|
| Fig.1.18 $C(u-u_0)$ is translated by $u_0=40$ toward the origin to give $C(u)$ | 29 |
| Fig.1.19 The wrapped phase from $-\pi/2$ to $\pi/2$ | 30 |
| Fig.1.20 The partial unwrapped phase only from $-\pi$ to π | 30 |
| Fig.1.21 The partial unwrapped phase only from 0 to 2π | 31 |
| Fig.1.22 Comparison between surface profile (solid line) and calculated one (dot line)..... | 32 |
| Fig.1.23 The generated surface profile shape and the generated interference pattern..... | 33 |
| Fig.1.24 Intensity distribution of the fringes..... | 34 |
| Fig.1.25 The amplitude distribution in the frequency domain..... | 34 |
| Fig.1.26 The amplitude distribution in the frequency domain after being filtered..... | 35 |
| Fig.1.27: The wrapped phase in two dimensions..... | 35 |
| Fig.1.28 Partially unwrapped phase from $-\pi$ to π | 36 |
| Fig.1.29 Partially unwrapped phase from 0 to 2π | 37 |
| Fig.1.30 Unwrapped phase in two dimensions..... | 37 |
| Fig.1.31 Comparison between the calculated surface (a) and the original surface (b)..... | 38 |
| Fig.1.32 The flow chart of procedure of surface profile measurement by Takeda method and Kreis method..... | 39 |
| Fig.2.1 The fringe stabilization system..... | 41 |
| Fig.2.2 Choosing the optimal set-point and locking point..... | 43 |
| Fig.2.3 PID Controller Tuning Flow chart | 44 |
| Fig.2.4 Set up of the experiment of surface measurement..... | 45 |
| Fig.2.5 Comparison for intensity of PD between with stabilization and without stabilization..... | 52 |
| Fig.2.6 Comparison about the calculated surface profile of step height | |

| | |
|---|----|
| with (L) and without (R) stabilization..... | 53 |
| Fig.2.7 The result of measurement in 2D by Accura2000 system..... | 56 |
| Fig.2.8 The result of measurement in 3D by Accura2000 system..... | 56 |
| Fig.3.1 Energy level diagram of ^{85}Rb and ^{87}Rb showing the hyperfine structure of the $5S_{1/2}$, $5P_{1/2}$ and $5P_{3/2}$ level value in MHz..... | 61 |
| Fig.3.2 Intensity distribution of TEM_{00} (dark circle) and TEM_{10} (light ellipses) on the split photodiode..... | 63 |
| Fig.3.3 Vector summation of electric fields on each photodiode half with TEM_{00} | 64 |
| Fig.3.4 The optical block diagram about laser frequency stabilization using the regulator PID 100..... | 66 |
| Fig.3.5 Saturated absorption and error signals generated by the interferometer tilt-locking system, measured $^{85}\text{Rb } 5^2 S_{1/2}, F3-F'4 \rightarrow 5^2 P_{3/2}$ | 68 |
| Fig.3.6 Free running and PID locked laser frequency fluctuations from about 27s..... | 71 |
| Fig.4.1 (appendix) The front panel of PID 100..... | 80 |
| Fig.4.2 (appendix) Diode/Grating in Littrow configuration..... | 86 |

List of tables

| | |
|--|----|
| Table.2.1 Statistical parameters under the condition: without stabilization..... | 48 |
| Table.2.2 Statistical parameters under the condition: with stabilization..... | 48 |
| Table.2.3 Comparison of statistical parameters between the non-stabilization and stabilization..... | 49 |
| Table.2.4 Records of experiment about input voltage and displacement of mirror (1)..... | 50 |
| Table.2.5 Records of experiment about input voltage and displacement of mirror (2)..... | 51 |
| Table.2.6 Five group of calculated roughness amplitude parameters... | 55 |
| Table.2.7 The results of calculated roughness amplitude parameters.. | 55 |
| Table.2.8 The comparison of results between ours and commercial ones of the experiment | 58 |
| Table.3.1 Some features of Rubidium..... | 60 |
| Table.4.1 (appendix) Specifications of step height standard..... | 77 |
| Table.4.2 (appendix) Specifications of laser source..... | 77 |
| Table.4.3 (appendix) Specifications of PIEZO Controller..... | 78 |
| Table.4.4 (appendix) Specifications of photo Diode Amplifier with switchable gain..... | 79 |
| Table.4.5 (appendix) Specifications of photo detectors..... | 79 |
| Table.4.6 (appendix) Specifications of the Oscilloscope..... | 80 |
| Table.4.7 (appendix) Specification of CCD camera..... | 82 |

Introduction

In the environmental lab conditions, there are many perturbations which can affect the results of the experiment, such as thermal drift, wind-flowing, mechanical vibrations on the table, etc. As a typical case, when a person passes by the table of the experiment, the environmental lab conditions will be disturbed heavily due to the wind and vibrations derived from the movement of the people. For the experiment of surface profile measurement, we must stabilize the interferometer so as to get an image of high quality.

The stabilization system is a closed loop of feedback which was proportional, integration and differential system. When the error signal due to external perturbations is detected by the silicon photo diode, it will be scaled and amplified by photo diode amplifier and enters into the PID controller. Through tuning the parameters including set point, integral, proportional and derivative etc, the output of PID controller will send a control signal to PZT controller. Having received the control signal, the PZT controller will drive the reference mirror which is adhered with the PZT transducer moving to correct the optical path changing derived from the perturbations until the error signal disappears.

Phase shifting method and Fast Fourier Transform method are two important methods in the field of non-contact surface profile measurement. For phase shifting method, because it changes the stabilization parameters whenever the reference mirror is moved for

phase shift, it is difficult to get the stabilization and phase shifting by changing the positions in reference path. However, the FFT method can overcome this disadvantage of phase shifting method. Because there is only one image of interference fringe pattern in FFT method instead of several images in phase shifting method, and it is possible to stabilize the measurement system.

First we did simulation FFT in 1D and 2D profile to confirm whether our generated mathcad codes are correct or not by using Takeda^[1] and Kreis method^[2]. So we used FFT method and stabilization of the interferometer together to process stabilized image in the harsh environmental conditions. We measured the reference step height with the thickness 93 nm in highly windy environmental conditions and compared this with measurement in stable conditions with commercial Mirau type interferometer.

In the second application of PID controller, we used it to the frequency stabilization of diode laser by using tilt locking^[3] method in Sagnac interferometer. In many applications of diode laser system, the frequency stabilization is very important. Compared with the traditional old methods, the tilt locking method is novel and has some extraordinary advantages. For example, tilt locking method don't need expensive components which are used in the old methods mentioned above such as acousto-optic modulators, electro-optic modulators, wave plates, or lock-in amplifiers etc^[4]. As two beam interferometer, the output of Sagnac interferometer can be described on the basis of TEM mode of

cavity modes^[3]. TEM_{00} mode and TEM_{01} mode are the electric fields of the first two Hermite–Gauss modes of cavity modes. In this experiment, an important task is to obtain the error signal as the reference. In the Sagnac interferometer, the rubidium vapor cell was positioned and the probe beam was scanned by SC100 system across the atomic resonance. Due to the relationship between the frequency, refractive index and phase changing, the changing of the refractive index of the atoms would lead to phase shift and the phase shift made the interference between the TEM_{00} mode and TEM_{01} mode from the cavity modes. Up to now, the error signal is obtained. The error signal was captured by commercial quadrant photodiode and passed the closed feedback loop which was set up by Sagnac interferometer and PID controller together. As the result, the laser frequency is stabilized up to sub-megahertz level in the experiment.

I. Stabilization of surface measurement with Fast Fourier Transform method by PID controller

1. The simulation of surface profile measurement by Fast Fourier Transform method.

1.1 Introduction of surface profile measurement technology by using Fast Fourier Transform method

The analysis of fringe pattern from the object has many industrial and medical applications.

There are many methods which can be used to analyze fringe patterns. In general, the phase stepping method, the Fast Fourier Transform (FFT) method and the direct phase detection method are mentioned at most cases^[5], and even in artworks field. First two methods are mainly used in practice. Interferometry is used broadly in the surface profile measurement. This technology has many applications in the measurement such as length measurement, surface measurement and vibration analysis, etc. We analyze the fringe-pattern because the information of the surface profile is embedded into the image. We used the technology of FFT method or the phase stepping method to obtain the phase map from the fringe-pattern. The phase map is derived from the optical path length difference between the object path and reference path. As the formula of calculation of the height, the height map will be obtained from the phase information finally.

Before introducing the methods about surface measurement, we should explain some basic knowledge about interference equations.

As electromagnetic wave, the optical wave can be described into the following equations:

$$\vec{E} = \vec{E}_0 \cdot \exp i(\vec{k} \cdot \vec{r} - \omega t + \varphi_0) \quad (1)$$

where ω is angular frequency of the optical wave, k is wave vector, E_0 is amplitude and φ_0 is initial phase angle.

Two electric fields can be described in the following equations:

$$\vec{E}_1 = \vec{E}_{10} \cdot \exp i(\vec{k} \cdot \vec{r}_1 - \omega t + \varphi_{10}) \quad (2)$$

$$\vec{E}_2 = \vec{E}_{20} \cdot \exp i(\vec{k} \cdot \vec{r}_2 - \omega t + \varphi_{20}) \quad (3)$$

The intensity due to two electric fields can be described as equation (4).

$$\begin{aligned} I &= (\vec{E}_1 + \vec{E}_2) \cdot (\vec{E}_1^* + \vec{E}_2^*) \\ &= E_{10}^2 + E_{20}^2 + 2E_{10}E_{20} \cos \Delta\varphi \\ &= A_1^2 + A_2^2 + 2A_1A_2 \cos \Delta\varphi \end{aligned} \quad (4)$$

$$\Delta\varphi = k \cdot (\vec{r}_1 - \vec{r}_2) + (\varphi_{10} - \varphi_{20}) \quad (5)$$

Thus, the fringe pattern originated from path difference between reference mirror and the object can be represented by the following equation:

$$I(x,y) = I_{dc} + I_{ac} \cos[\phi(x,y) + \phi(t)] \quad (6)$$

where I_{dc} represents the intensity of background, I_{ac} represents the intensity modulation bias, $\phi(x,y)$ represents the measured object phase

and $\phi(t)$ represents the phase shift. By changing the optical phase when we measured the interferogram, we get four measured interferogram intensity patterns as the following equations^[6]:

$$I_1(x,y)=I_{dc} + I_{ac}\cos[\phi(x,y)] \quad (7)$$

$$I_2(x,y)=I_{dc} + I_{ac}\cos[\phi(x,y)+ \pi/2] \quad (8)$$

$$I_3(x,y)=I_{dc} + I_{ac}\cos[\phi(x,y)+ \pi] \quad (9)$$

$$I_4(x,y)=I_{dc} + I_{ac}\cos[\phi(x,y)+ 3\pi/2] \quad (10)$$

Thus we can work out the following phase from those four equations:

$$\phi(x,y)=\tan^{-1}\{[I_4(x,y)- I_2(x,y)]/[I_1(x,y)- I_3(x,y)]\} \quad (11)$$

Finally, the height map $h(x,y)$ of the object can be obtained with the measured optical phase.

$$h(x,y)=(\lambda/4\pi)* \phi(x,y)^{[7]} \quad (12)$$

Above we reviewed the phase stepping (four step) method for surface measurement. The phase stepping technology requires either three, four images, etc. to extract the phase information.

Compared with the phase stepping method, the FFT method requires only one fringe pattern in order to obtain information of the surface profile.

Now we introduce the fast Fourier transform method.

The Fourier transform and the inverse Fourier transform for functions $g(x)$ and $G(u)$ are given in the following, respectively^[8]:

$$G(u) = \int_{-\infty}^{\infty} g(x) \exp(-j2\pi ux) \quad (13)$$

$$g(x) = \int_{-\infty}^{\infty} G(u) \exp(j2\pi ux)$$

For discrete transform such transformations can be defined as:

$$G(n) = \frac{1}{N} \sum_{k=0}^{N-1} g(k) \exp(-j \frac{2\pi nk}{N}) \quad (14)$$

$$g(k) = \sum_{n=0}^{N-1} G(n) \exp(j \frac{2\pi nk}{N}) \quad (15)$$

In the various optical measurements, the fringe patterns can also be represented by the following equation^[8]:

$$f(x,y) = a(x,y) + b(x,y) \cos[2\pi u_0 x + \phi(x,y)] \quad (16)$$

where $a(x,y)$ and $b(x,y)$ are the intensity of background and modulation bias, respectively, and the phase $\phi(x,y)$ contains the information about the surface profile which we desired. Also u_0 is spatial frequency of the carrier fringes in x -direction and we do not need consider y -direction spatial frequency because there are no y -components of the fringe modulation. The interferogram can also be written in complex form^[8]:

$$f(x,y) = a(x,y) + (1/2)b(x,y) \{ \cos[2\pi u_0 x + \phi(x,y)] + j \sin[2\pi u_0 x + \phi(x,y)] + \cos[2\pi u_0 x + \phi(x,y)] - j \sin[2\pi u_0 x + \phi(x,y)] \} \quad (17)$$

Where $\cos[2\pi u_0 x + \phi(x,y)] - j \sin[2\pi u_0 x + \phi(x,y)]$ is complex conjugate.

Eq (17) can be written in a more convenient form^[8]:

$$f(x,y) = a(x,y) + (1/2)b(x,y) \{ \exp[j\phi(x,y)] \exp[j2\pi u_0 x] + \exp[-j\phi(x,y)] \exp[-j2\pi u_0 x] \} \quad (18)$$

Letting $c(x,y)=(1/2)b(x,y)\exp[j\phi(x,y)]$, and $c^*(x,y)$ is its complex conjugate, and obtain the following Eq.(19)^[8]

$$f(x,y)=a(x,y)+ c(x,y)\exp(j2\pi u_0x)+ c^*(x,y)\exp(-j2\pi u_0x) \quad (19)$$

The FFT of $f(x,y)$ with respect to x direction would be^[8]:

$$F(u,y)=A(u,y)+ C(u-u_0, y)+ C^*(u+ u_0, y) \quad (20)$$

In the frequency domain, spectra $A(u,y)$ and $C^*(u-u_0,y)$ are removed by band-pass filtering, and isolated the function $C(u-u_0,y)$, translated it by u_0 to the origin to obtain $C(u,y)$, and computed the inverse Fourier transform of $C(u,y)$ to obtain $c(x,y)$.

In Eq.(21), the function $A(u,y)$ represents the contribution to the spectra from low-frequency background illumination. $C(u-u_0,y)$ and $C^*(u+ u_0,y)$ are centered around $u= u_0$ and $u=- u_0$.

Thus, in one dimension, spectra $A(u)$ and $C^*(u+ u_0)$ are filtered by band-pass filtering. We got the function $C(u-u_0)$, which is subsequently translated by u_0 toward the origin so as to get $C(u)$.

By applying the inverse Fourier transform, $c(x)$ is obtained^[8]:

$$c(x,y)=(1/2)b(x,y)\exp[j\phi(x,y)] \quad (21)$$

From the above equation, the phase can be calculated by inverting the relation Eq.(22)^[8]:

$$\tan[\phi(x,y)]=\text{Im}[c(x,y)]/\text{Re}[c(x,y)] \quad (22)$$

$$\phi(x,y)=\arctan\{ \text{Im}[c(x,y)]/\text{Re}[c(x,y)]\}^{[9]} \quad (23)$$

Where Im and Re denote the imaginary and real parts of $c(x,y)$, respectively.

Because the phase calculated by Eq.(28) is wrapped between $-\pi/2$ and $\pi/2$, it is necessary to unwrap the wrapped phase so that we can reconstruct the continuous phase function $\Phi(x,y)$.

Finally, the height of surface profile can be calculated by the following equation (12):

$$h(x,y) = (\lambda/4\pi) * \phi(x,y) \quad [7]$$

In the procedure introduced above, the unwrapping procedure is not easy, it is essential to explain in details.

From Eq.(28), what we got is not a continuous phases. They are inverse tangent values which are wrapped between $-\pi/2$ and $\pi/2$.

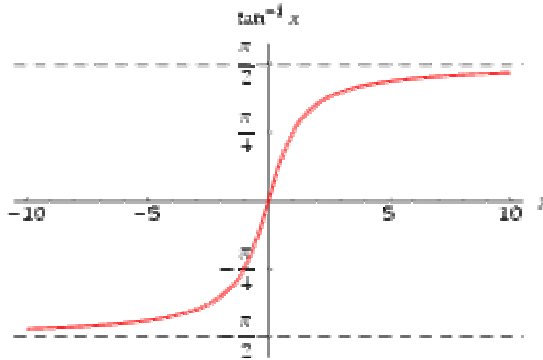


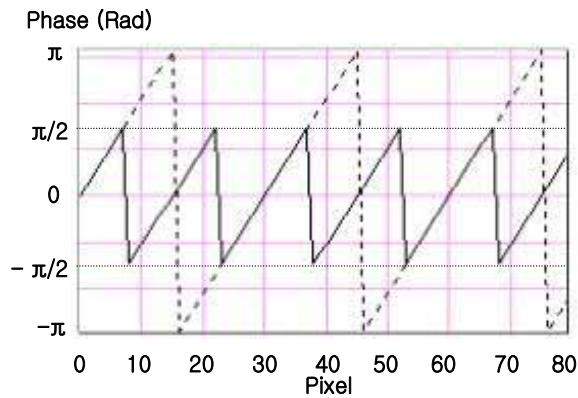
Fig.1.1 The graph of inverse tangent function

From Fig.1.1, about the inverse tangent function, there is always a unique solution between $-\pi/2$ and $\pi/2$. Because this is a wrapped phase, we should applied the phase unwrapping technology to solve this problem.

First, due to $\tan(x) = \sin(x)/\cos(x)$, we need unwrap the range of value from $\pi(-\pi/2 \sim \pi/2)$ modulo into $2\pi(-\pi \sim \pi)$ modulo, and then unwrap it to $0 \sim 2\pi$.

| | | | |
|------------|------------|--------------|--------------|
| | sin | | |
| cos | | + | - |
| + | | ϕ | ϕ |
| - | | $\phi + \pi$ | $\phi - \pi$ |

(a)



(b)

Fig.1.2 Unwrap the inverse tangent function from π modulo into 2π modulo.

Fig.1.2(a) demonstrates how to unwrap the phase from π modulo to 2π modulo. From the following equation, we can deduce the correct result.

$$\arctan(x) = \arcsin\left[\frac{\sin(x)}{\cos(x)}\right] \quad (24)$$

The value of inverse tangent function depends on the value of sine function and cosine function. In the coordinate system, x and y axis divide the space of coordinate into four parts which are named the first quadrant, the second quadrant, the third quadrant and the fourth quadrant, respectively. In the first quadrant, both of the value of sine function and cosine function are positive, so the values of tangent function and inverse tangent function are positive.

The value of inverse tangent do not need be changed. In the second quadrant, the value of sine function is positive while the value of cosine function is minus, so the value of tangent function and inverse tangent function are minus, in order to unwrap the phase value from π modulo to 2π modulo, we should add π to the value of inverse tangent function. In the third quadrant, both of the value of sine function and cosine function are minus, so the values of tangent function and inverse tangent function are positive, in order to unwrap the phase value from π modulo to 2π modulo, we should subtract π to the value of inverse tangent function. In the fourth quadrant, the value of sine function is minus and the value of cosine function is positive, both of the values of tangent function and inverse tangent function are minus. The value of inverse tangent need not be changed. Above results are shown in Fig.1.2 (a).

In order to avoid the phenomena of aliasing and eliminate the ambiguity, the absolute value of the subtraction between the phase of any point and its adjacent point must less than π . When the absolute value of

the subtraction between the phase of any point and its adjacent point is greater than π , it should be unwrapped (add or subtract 2π) so as to get the continuous phase distribution.

Above what we introduced is the basic theory of unwrapping phase procedure.

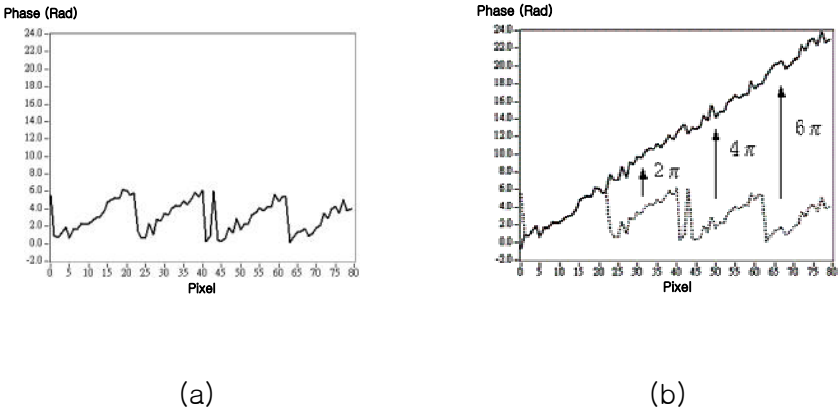


Fig.1.3 (a): Wrapped phase, the range of value is restricted in π modulo.

(b): Unwrapped phase by estimating the point of phase jump.

The following figure shows the unwrapping program algorithm which we used.

Unwrapping program flow chart in one dimension

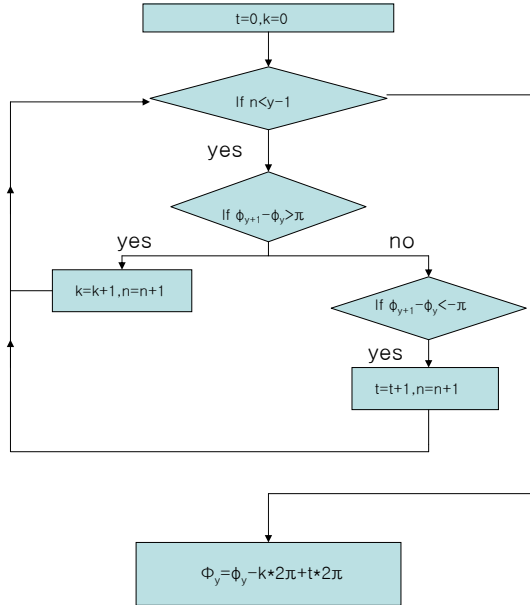
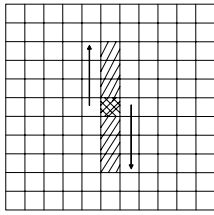


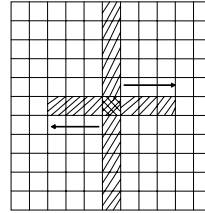
Fig.1.4: Unwrapping program flow chart in one dimension

The phase unwrapping procedure in two dimensions based on the case in one dimension, only some details should be emphasized.

The Fig.1.4 demonstrates the concept of path dependent unwrapping algorithm.



(a)



(b)

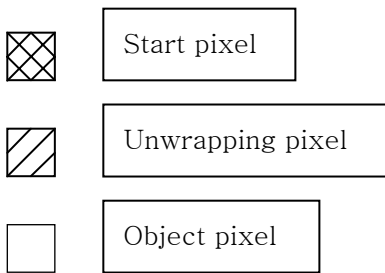


Fig.1.5: The concept of path dependent unwrapping algorithm in two dimensions

About phase unwrapping in two dimensions, the procedure is similar to that in one dimension, after selecting a starting point of unwrapping and as the following procedure to unwrap the phases. In general, the center point is selected, and we begin unwrapping the phases on the first row from the central point in y -direction. The path of unwrapping is shown in Fig.1.5 (a). Then, based on the unwrapped phases of central row

as the reference, we start unwrapping the phases on the rows in x-direction one by one. Finally, all of the phases in two dimensions will be unwrapped. The details are shown in the following sentences. First, we should select the start pixel as the reference pixel, give it position $P(i,j)$, and compare the value between the $P(i,j)$ and its adjacent pixel $P(i-1,j)$ and $P(i+1,j)$ respectively. If the absolute value of difference value between $P(i,j)$ and $P(i-1,j)$ or $P(i+1,j)$ is less than π , the value on $P(i-1,j)$ or $P(i+1,j)$ will be not changed. if the absolute value of difference value between $P(i,j)$ and $P(i-1,j)$ or $P(i+1,j)$ is greater than π , the phase value on $P(i-1,j)$ or $P(i+1,j)$ should be add or subtract 2π . The direction of unwrapping is shown on the figures. After finishing unwrapping the phases on the first row which includes the starting pixel, we should check the absolute value between the starting pixel $P(i,j)$ and $P(i,j-1)$ or $P(i,j+1)$, if the absolute value of difference value between $P(i,j)$ and $P(i,j-1)$ or $P(i,j+1)$ is less than π , the value on $P(i,j-1)$ or $P(i,j+1)$ will be not changed. If the absolute value of difference between $P(i,j)$ and $P(i,j-1)$ or $P(i,j+1)$ is greater than π , the phase value on $P(i,j-1)$ or $P(i,j+1)$ should be add or subtract 2π . Then we can set the wrapped phases on the first row as the reference, unwrap the values on the other rows in x-direction as the direction which is shown by the arrow on the Fig.1.5 (b).

Now, combining a simulated case of one dimension, we demonstrate the FFT method of surface profile measurement.

1.2 The simulation of the profile measurement in one-dimension.

In this case, we used the mathcad software to develop a program to simulate the procedure of surface profile measurement by FFT method.

There are two methods about analyzing the fringe-pattern in practice by using FFT method. One is Kreis method^[2], another one is Takeda method^[1]. In this case, we will introduce two methods, respectively.

When we use the Kreis method^[2] to analyze the fringe-pattern, we should divide the data obtained after FFT into three parts. First part is the component of the background and the second part is the component of the low frequency, and the third part is the component of the high component in the frequency domain. By eliminating the components of the background illumination and the high frequency, we will get the component of the low frequency only, then the contour can be reproduced using the inverse Fourier transform and phase unwrapping techniques.

The second method is Takeda method^[1]. By using the Takeda method, the Fourier transform method for fringe pattern analysis requires an added spatial-carrier frequency, the sinusoidal fringes derived from the plane surface serve as the carrier. If the spatial carrier frequency is properly selected, the contour can be reproduced using the inverse Fourier transform and phase unwrapping techniques. More details will be explained in the following simulated cases.

The heart of optical system for surface measurement is interferometry. It is essential to introduce the setup of Twyman-Green interferometry.

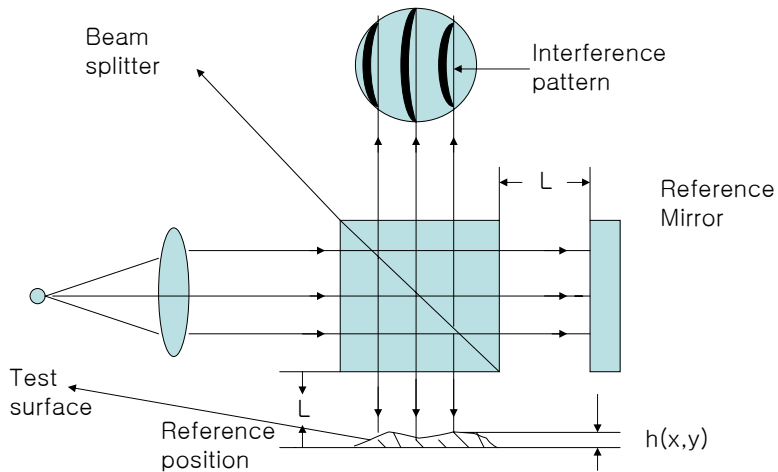


Fig.1.6: Twyman-Green interferometry

In the optical system of the interferometer, the laser beam comes from the source, at first. It passes through the beam splitter, one beam transmitted beam splitter. Another one is reflected and goes to the test surface. Then the transmitted beam would be reflected by the reference mirror and passed through the beam splitter secondly. This beam also was divided into transmitted part and reflected part. Simultaneously, the reflected beam passed through the beam splitter again too. It would be divided into reflected part and transmitted part also. Finally, there were two beams projected on the screen, one came from test surface and

another one came from reference mirror. Two beams are combined and formed fringe pattern on the screen. When the laser beams are projected onto a surface, there is the fringe-pattern formed due to the optical path difference. Then the surface profile, acts as a phase modulator. The amount of modulation at any point depends on the height of the surface profile at that point.

The wavefront of reflected reference is

$$W_r(x,y)=A^* \exp(2jkl) \quad (25)$$

The wavefront of reflected test surface is

$$W_t(x,y)=B^* \exp[2jk(l-h(x,y))] \quad (26)$$

Then, the interference pattern is described as

$$\begin{aligned} I(x,y) &= |W_r(x,y) + W_t(x,y)|^2 \\ &= |A^* \exp(2jkl) + B^* \exp[2jk(l-h(x,y))]|^2 \\ &= a^2 + b^2 + 2ab \cos[2kh(x,y)] \\ &= I_o(1 + \gamma \cos \phi(x,y)) \end{aligned} \quad (27)$$

where a and b denote the wavefront amplitude,

$k=2\pi/\lambda$: propagation number

$$\phi(x,y)=2kh(x,y) \quad [10]$$

Above we discussed principle of the surface measurement with FFT method by Twyman-Green interferometry. Now we introduce a program to calculate the surface profile^[11].

Because it is a simulated case, we should generate a surface profile function first. The generated surface profile is shown on the following figure:

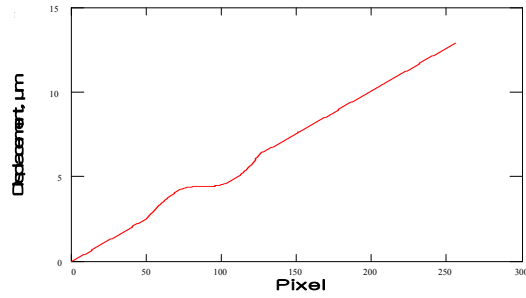


Fig.1.7: The graph of the surface profile function, the surface is tilted in a small angle.

There is the interference pattern which is derived from the contour of surface profile.

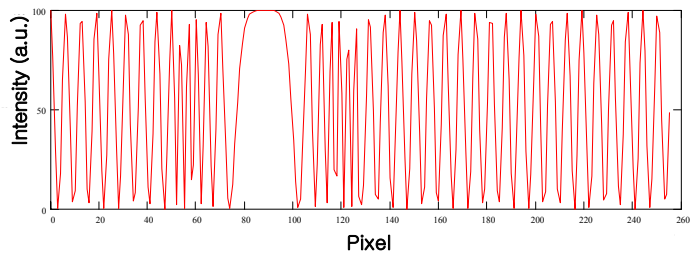


Fig.1.8: The intensity function of interference pattern

We can read the data from the above graph and process the data by FFT.

Let's analyze the data from the spatial domain into the frequency domain.

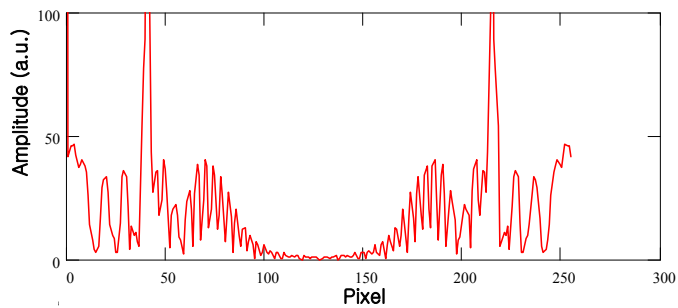


Fig.1.9: The amplitude distribution in the frequency domain after FFT

Analyze the fringe-pattern in two methods: the Kreis method^[2] and the Takeda method^[1].

The first one being introduced is Kreis method^[2]:

From Fig.1.8, we found the graph could be divided into three parts.

The first part is the component of background, its value is the biggest in the frequency domain. The second part is the component of the low frequency. The third part is the components of the high frequency. We design a filter to eliminate the components of background and high

frequency.

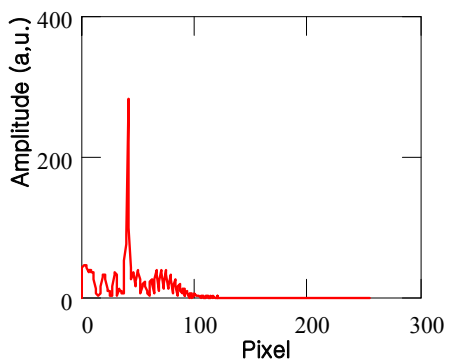


Fig.1.10: The graph of the low frequency component

After processing the data by IFFT, we got the real part and the imaginary part of the complex number, respectively and the value of inverse tangent function would be obtained.

Fig.1.11 shows the origin wrapped phase.

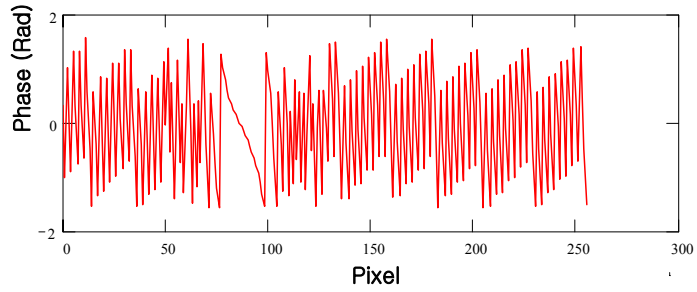


Fig.1.11: The wrapped phase from $-\pi/2$ to $\pi/2$

Because the interval of the principal value of the inverse tangent function is from $-\pi/2$ to $\pi/2$, we should unwrap the phases from modulo π to modulo 2π first.

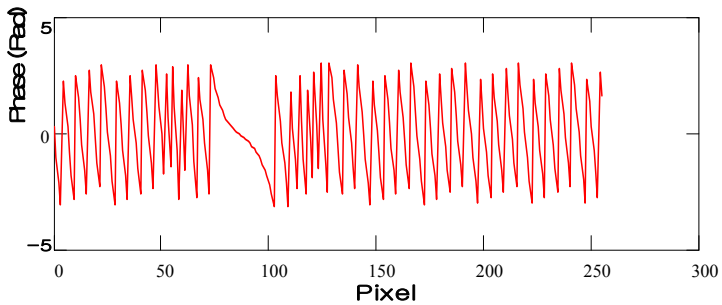


Fig.1.12: The partial unwrapped phase only from $-\pi$ to π

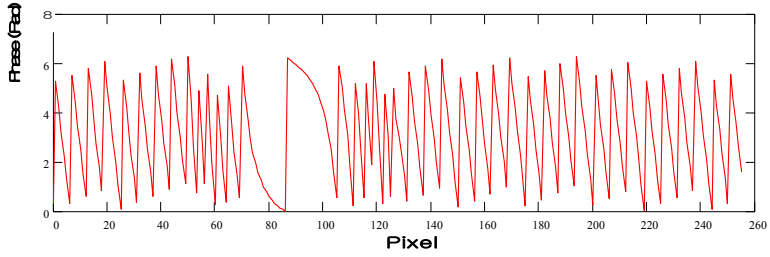


Fig.1.13: The partial unwrapped phase only from 0 to 2π

Finally, we developed a program to unwrap and normalize the phases and got the consistent unwrapped phases. We can get the height of the surface profile by Eq (12):

$$H(x) = (\lambda/4\pi) * \phi(x)$$

Unit of lamda is nm, $\lambda = 632.8$

We compared the graphs between the result which we calculated and the surface profile of origin.

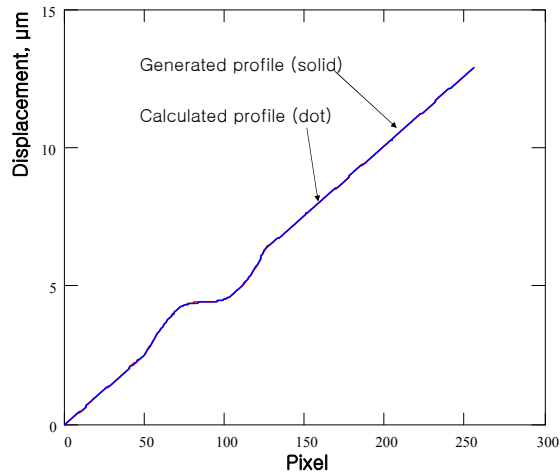
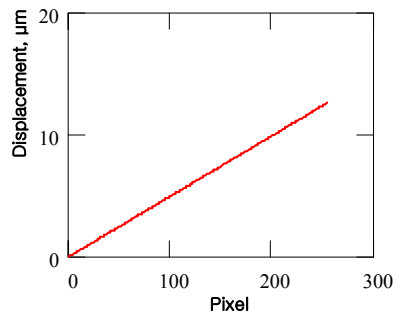


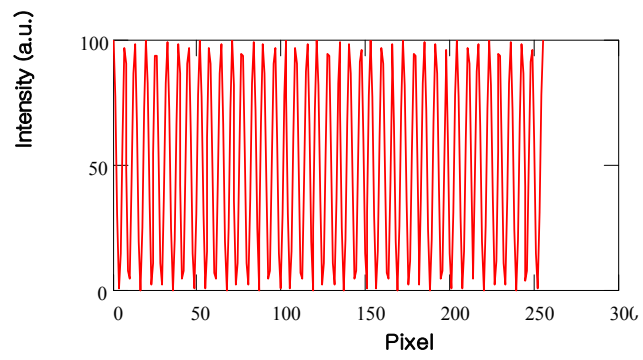
Fig.1.14: Comparison between the original profile and the calculated profile

The following program is for Takeda method^[1].

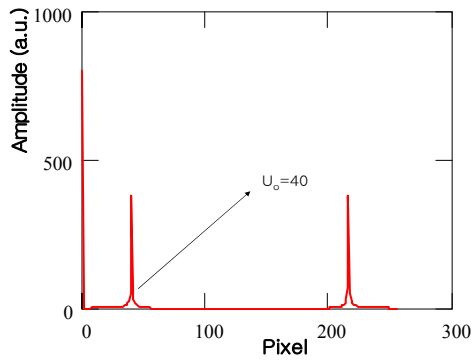
The first step is to find out the carrier frequency u_0 . U_0 is the spatial frequency of interference fringe pattern which is calculated in the following method. We generated a plane surface and got the fringe pattern, after FFT, we got the carrier frequency $u_0=40$ from the fringe pattern of our generated plane surface.



(a)



(b)



(c)

Fig.1.15: (a): Plane surface

(b): Interference for plane surface

(c): Get the carrier frequency from frequency domain

Having gotten the carrier frequency $u_0=40$, we processed the data which were obtained by FFT with Takeda method^[1].

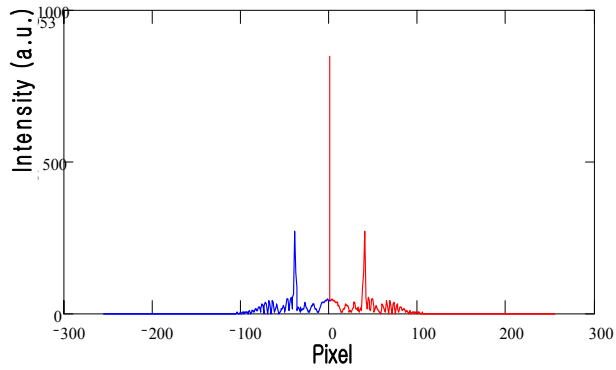


Fig.1.16: $C(u-u_0)$ and $C^*(u+u_0)$ are centered around $u= u_0$ and $u=- u_0$.

We can see the function $A(u)$ represents the contribution to the spectra from low frequency background illumination and it is centered around $u=0$, and $C(u-u_0)$ and $C^*(u+u_0)$ are centered around $u= u_0$ and $u=-u_0$.^[7]

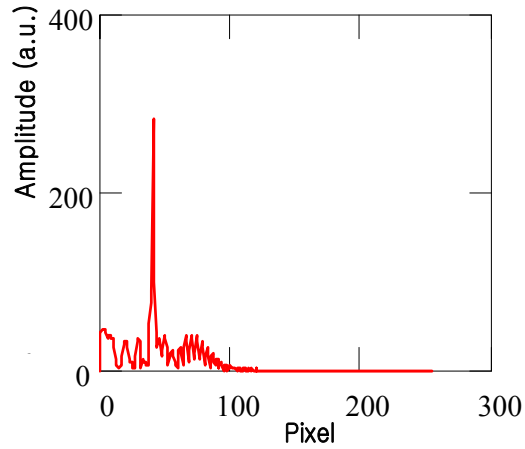


Fig.1.17: Function $C(u-u_0)$

Fig.1.17 showed that Spectra $A(u)$ and $C^*(u+u_0)$ were eliminated by band pass filtering, thus isolated the function $C(u-u_0)$.

The spectra would be shifted in the frequency domain. $C(u-u_0)$ was translated by $u_0 = 40$ toward the origin to give $C(u)$.

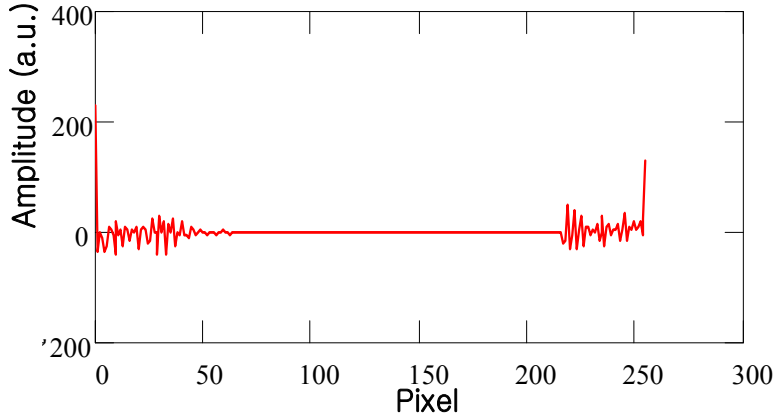


Fig.1.18: $C(u-u_0)$ is translated by $u_0 = 40$ toward the origin to give $C(u)$.

Having obtained $C(u)$, IFFT was used to get the $c(x)$ in the spatial domain.

The real part and the imaginary part of the complex number would be obtained respectively after IFFT.

$$\tan[\phi(x)] = \text{Im}[c(x)]/\text{Re}[c(x)] \quad (22)$$

$$\phi(x) = \arctan\{\text{Im}[c(x)]/\text{Re}[c(x)]\} \quad (23)$$

The values of inverse tangent function which were obtained by Eq.(23) are shown in Fig.1.19.

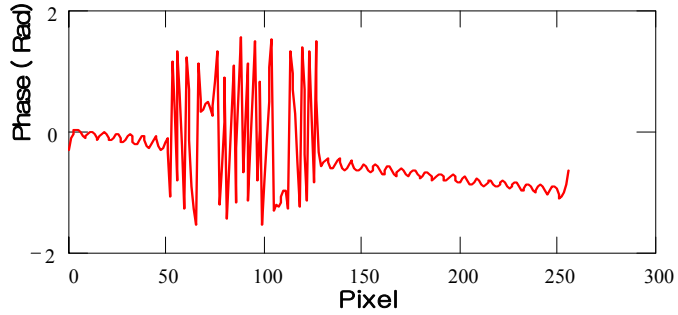


Fig.1.19: The wrapped phase from $-\pi/2$ to $\pi/2$.

The following procedure is same as the Kreis method^[2]. We unwrap the wrapped phases from π modulo into 2π modulo first.

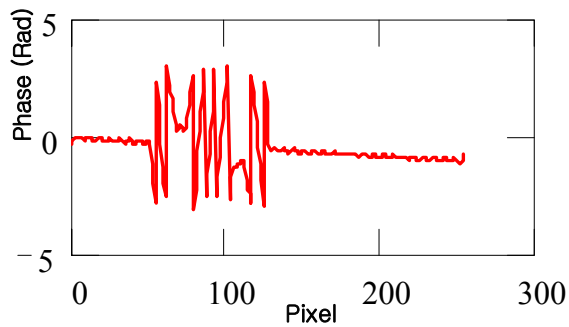


Fig.1.20: The partial unwrapped phase only from $-\pi$ to π

Then unwrap the phases from 0 to 2π .

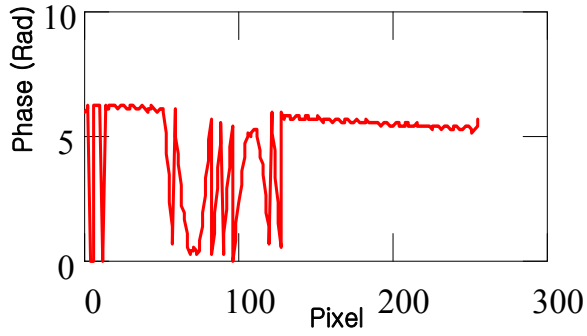


Fig.1.21: The partial unwrapped phase only from 0 to 2π

Finally, we developed a program to unwrap and normalize phases entirely, and the consistent unwrapped phase would be obtained.

The height of the point on the surface profile would be extracted from the unwrapped phase data as Eq.(12):

$$H(x) = (\lambda/4\pi) * \phi(x)$$

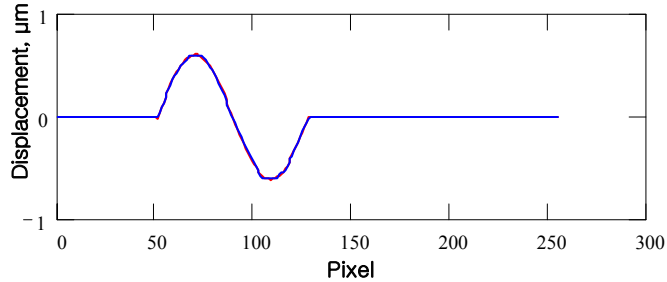


Fig. 1.22: Comparison between generated surface profile (solid line) and calculated one (dot line)

1. Discussion and Conclusion:

From the above introduction, we had simulated the measurement of surface profile by FFT in mathcad successfully.

Comparing between the original function and the calculated profile, we found the calculated profiles were match to the original surface profile very exactly.

By analyzing the procedure of calculating the surface profile we can draw the following conclusions. Whether the surface profile is regular or not, it's no question to be calculate by FFT method. In fact, the information of surface profile is encoded into the interference fringe pattern, analyzing the interference pattern is our main task. Image

processing has been an important technique in non-contact surface profile measurement field.

1.3 The simulation of the surface profile measurement in two-dimensions

After introducing the program about the surface profile measurement in one dimension, we tried to develop another program to measure the surface profile in two dimensions^[11].

In this case, we generated a near spherical surface and got the fringe pattern, as the steps which were introduced in Chapter 1.1.

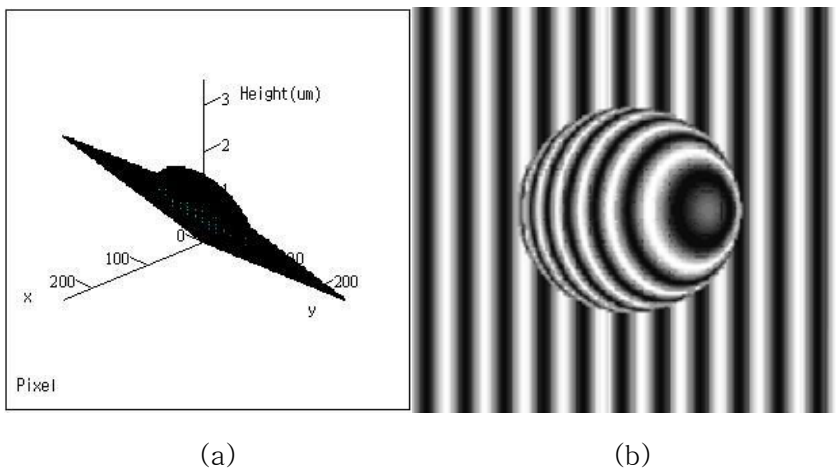


Fig.1.23: The generated surface profile shape and the generated interference pattern.

In Fig.1.23 (a), a near sphere profile shape was generated. Fig.1.23 (b) shows the generated interference pattern in Twyman-Green interferometer and the pattern encoded the information of the near sphere profile shape.

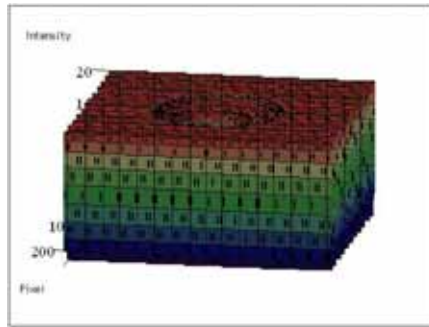


Fig.1.24: Intensity distribution of the fringes

In Fig.1.24, the intensity distribution of the interference pattern was generated, the same as the interference fringe pattern, it is also encoded the information of surface profile.

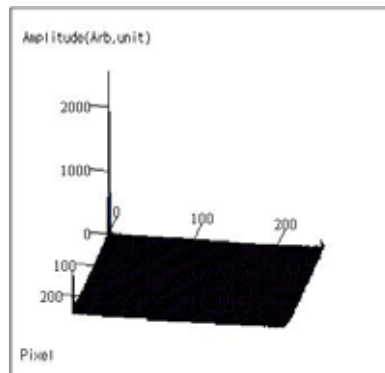


Fig.1.25: The amplitude distribution in the frequency domain

Fig.1.25 shows the magnitude of FFT in the frequency domain.

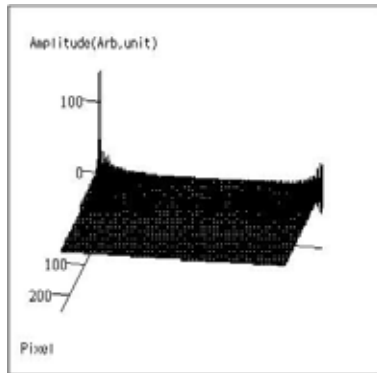


Fig.1.26: The amplitude distribution in the frequency domain after being filtered

After being filtered by band pass filter, the components of low frequency were isolated and the components of background and high frequency are eliminated in frequency domain.

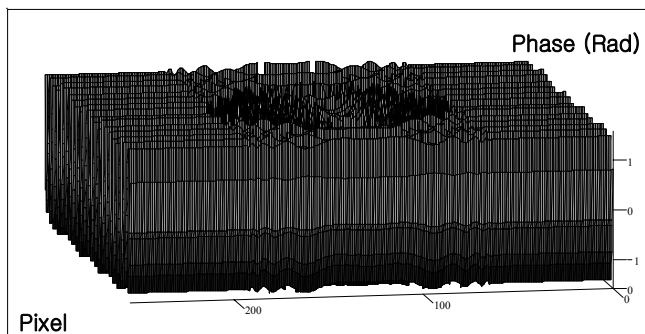


Fig.1.27: The wrapped phase in two dimensions

Fig.1.27 shows the wrapped phases which are obtained after IFFT. Because the data which are obtained after IFFT are complex numbers,

the information of phases is encoded into the imaginary part and the real part of the complex numbers. By Eq.(22) and Eq.(23), the wrapped phases are obtained finally.

As shown in Fig.1.28, facing up to the wrapped phases, we should unwrap the phases from π modulo into 2π modulo first.

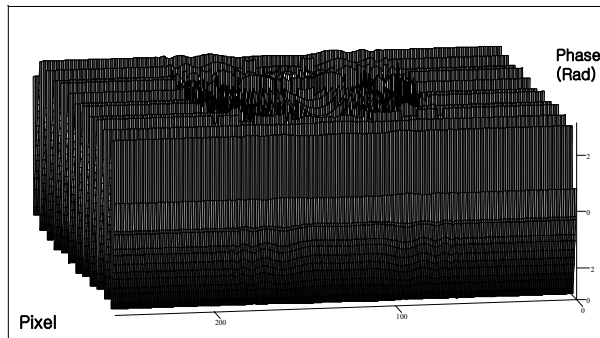


Fig.1.28: Partially unwrapped phase from $-\pi$ to π

The phases which are obtained and shown in Fig.1.28 are including positive and minus numbers, however, in order to calculate the final profile, we need only the positive numbers. It is necessary to unwrap the phases from interval $-\pi \sim \pi$ into interval $0 \sim 2\pi$. Fig.1.29 shows this result.

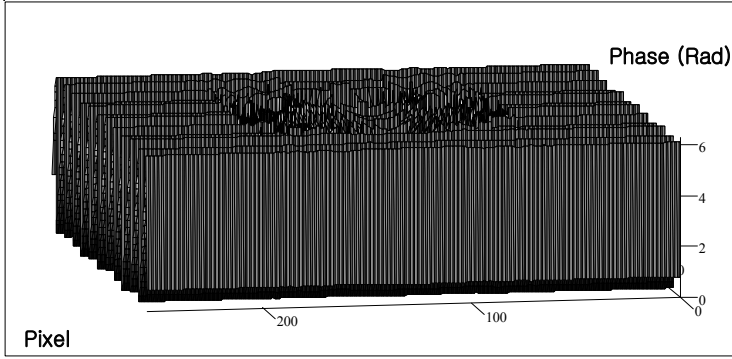


Fig.1.29: Partially unwrapped phase from 0 to 2π

After obtaining the phases from 0 to 2π , it is important to develop a program to unwrap and normalize the phases so that we can get the consistent phases which is shown in Fig.1.30.

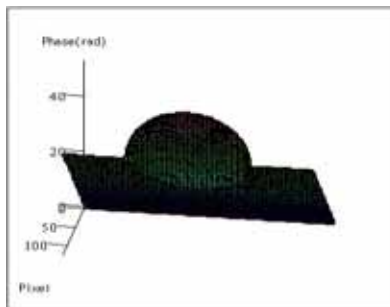


Fig.1.30: Unwrapped phase in two dimensions

Having gotten the unwrapped phases, we can use the Eq.(12) to

calculate the height utilizing the relationship between height, phase and wavelength λ .

$$h(x, y) = \left(\frac{\lambda}{4\pi}\right) \cdot \phi(x, y) \quad (12)$$

Fig.1.31 shows the comparison between the calculated surface and the original generated surface. We found the calculated surface profile agrees well with the original surface profile^[12].

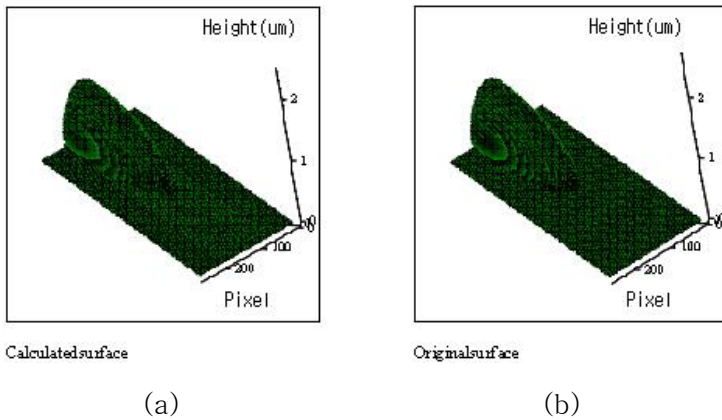


Fig.1.31: Comparison between the calculated surface (a) and the original surface (b).

Summarizing of the above simulations about surface profile measurement by FFT method in one dimension and two dimensions, we found the FFT method has many advantages over phase shift method. Only one image is needed in FFT method, while several images are needed in phase shift method. Either Takeda method^[1] or Kreis method^[2] is proved to simulate the procedure of surface profile measurement successfully. We made a Figure of flow chart to summary Takeda method^[1] and Kreis method^[2].

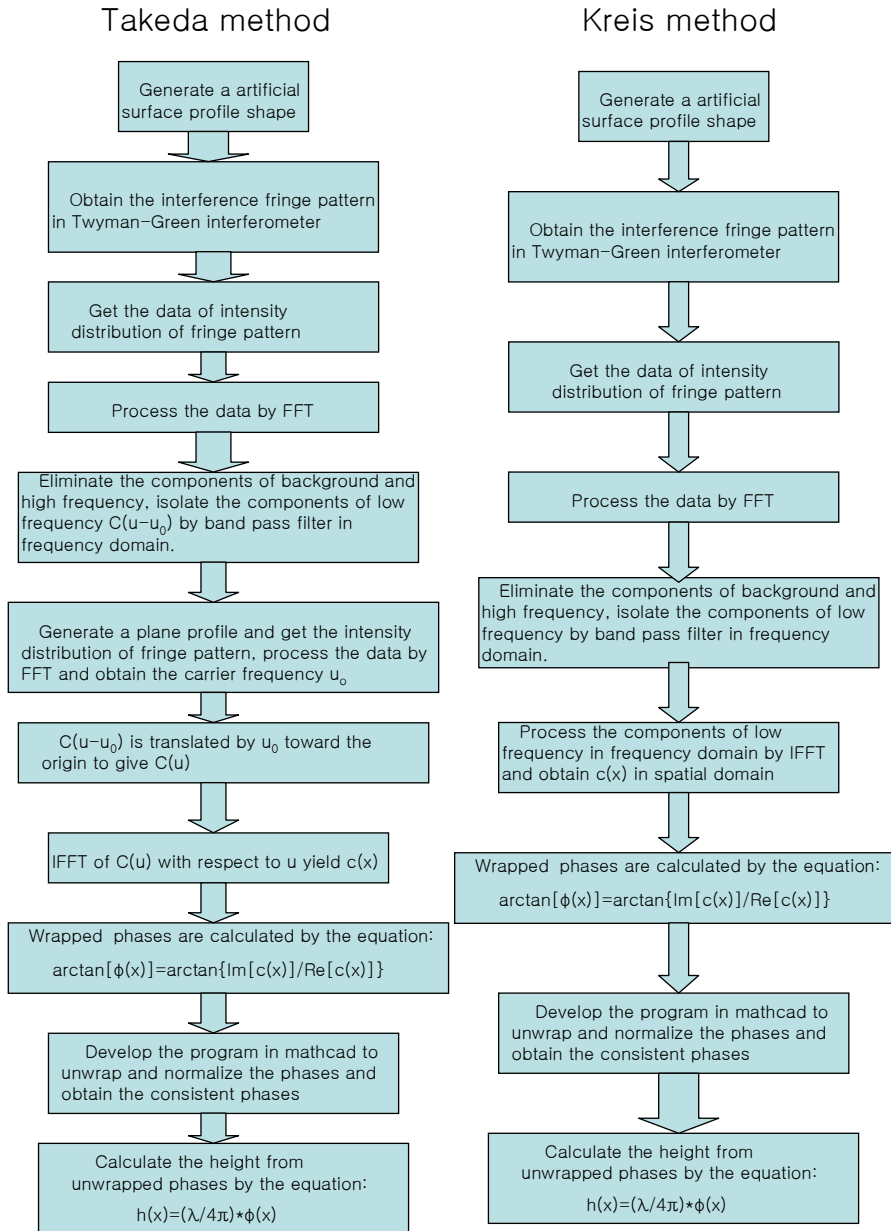


Fig.1.32: The flow chart of procedure of surface profile measurement by Takeda method^[1] and Kreis method^[2]

2. The experiment and analysis of stabilization of surface profile (step height) measurement with Fast Fourier transform method by PID controller

2.1 Introduction of PID controller

In general, there are the PID control, the ratio control, the logical control and so on the many kinds of controls algorithm. In the field about closed feedback loop control system, the PID control systems are used in most cases. We have mentioned that we used the commercial stabilock II^[13] active fringe stabilizer system to stabilize the interferometer before. In fact, both of PID controller system and stabilock II^[13] system work on the interferometer-mirror-piezo system, measure the error signal with detector and correct optical path difference with piezoelectric. The difference between them is only on the different means to get the error signal. In the PID control system, the error signal derived from the difference between the measurement voltage and the set point voltage because there is only one photo diode in the interferometer. Whereas, in the stabilock II^[13] system, the error signal is derived from the difference between two electronic signals which are scaled and amplified by two sense elements inside the detector head. The error signal is fed to the input of PID controller and PZT controller or stabilock II^[13] electronics control in the closed feedback system. The output signal which comes from the PZT controller or stabilock II^[13] electronics control will drive the reference mirror which is adhered with PZT transducer or piezo-electric bimorph moving so as to correct the optical path difference until

the fringe error (movement) disappears.

The fringe stabilization system consists of three basic components^[13].

1. The phase detector that senses the fringe movement.
2. Electronic board to control a feedback signal that is an error voltage proportional to the fringe movement.
3. PZT control system which corrects the relative optical path difference of the two beams in proportional to the error signal.

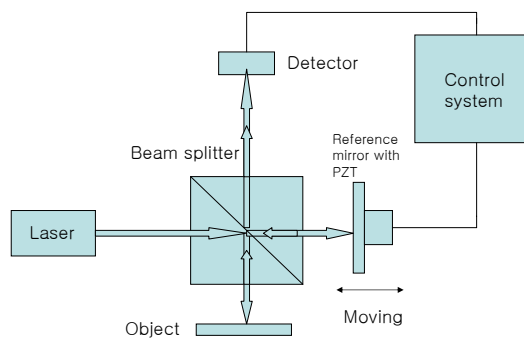


Fig.2.1: The fringe stabilization system

For the stabilization of the interferometers we used PID feedback control system. Fig.2.1 shows such an experimental system we used. There is only one photodiode in the PID control system. In the PID system, the set point is the locking voltage which we want to fix. The error signal is defined as the difference between the set point voltage and

input voltage to the PID system.

The output of PID controller will change in response to a change in input voltage or set point voltage.

About the P, I, and D, we introduce some definitions in the following:

Proportional term: with proportional term, the controller output is proportional to the error or a change in measurement, in the Eq.(31), the proportional output is denoted by parameter K_c ^[14].

Integral term: with integral action, the controller output is proportional to the amount of time that the error is present. Integral action eliminates offset^[15].

$$Output = \frac{1}{\tau_I} \int_0^t e(t) dt \quad (28)$$

Derivative: with derivative action, the controller output is proportional to rate of change of the measurement or error. The controller output is calculated by the rate of change of the measurement with time^[15].

$$Output = \tau_D \frac{de(t)}{dt} \quad (29)$$

where m is the measurement at time t .^[15]

Combining the functions about three factors about P, I and D, the PID controller is expressed by the following function^[14]:

$$p(t) = \bar{p} + K_c \left[e(t) + \frac{1}{\tau_I} \int_0^t e(t) dt - \tau_D \frac{de(t)}{dt} \right] \quad (30)$$

K_C is the gain parameter about P, τ_I is the time parameter about I and τ_D

is the time parameter about D.

It is important to choose the locking point on the line which is in steepest slope for tight locking.

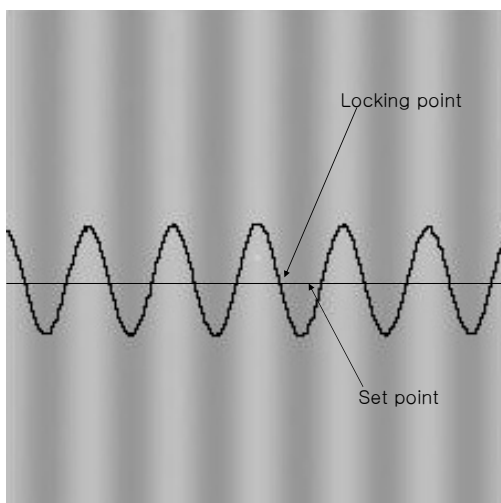


Fig.2.2: Choosing the optimal set point and locking point.

We made a flow chart to demonstrate the tuning procedure of PID controller to stabilize the fringes.

PID Controller Tuning Flow chart

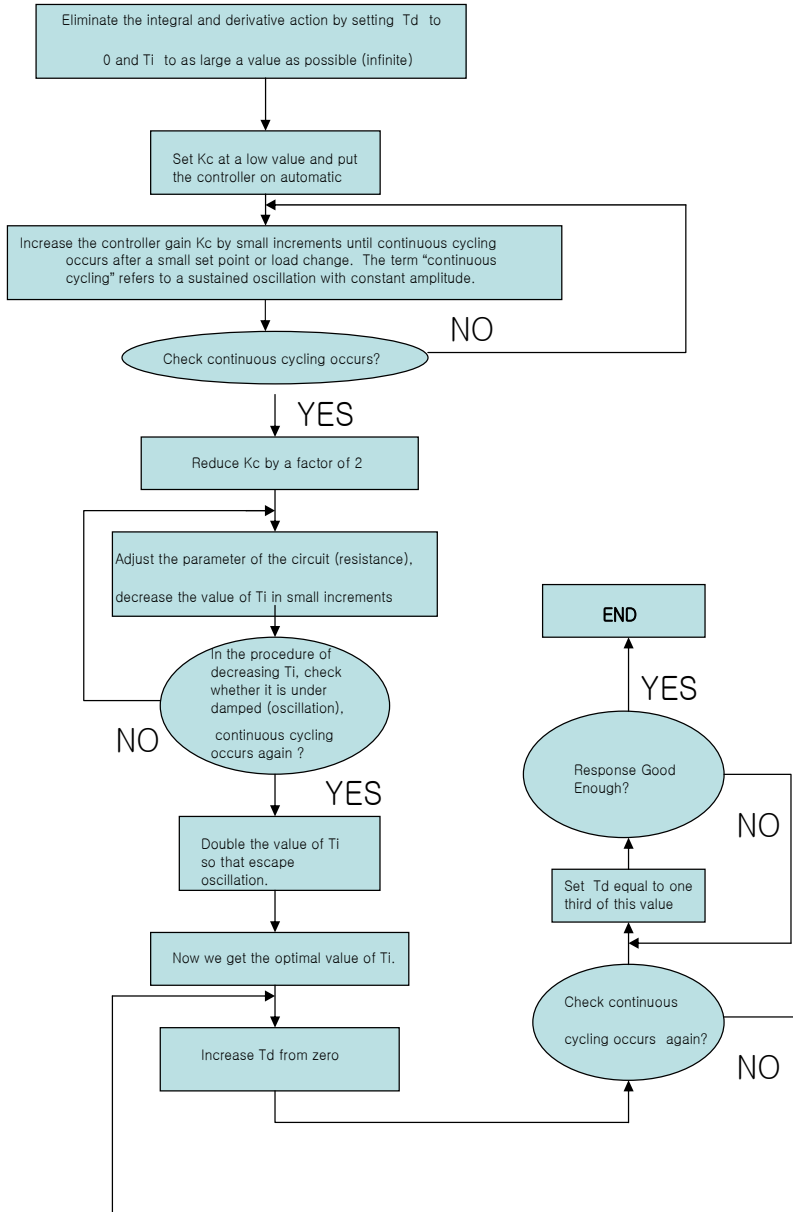


Fig.2.3: PID Controller Tuning Flow chart

2.2 Introduction of experiment

In this experiment, we set up a Twyman-Green interferometer to measure the step height. We connected the interferometer to the PID controller and PZT controller to buildup a closed feedback loop. And we captured the image from the monitor of the computer which is connected with the CCD camera.

All of the models of components in the experiment are shown in the appendix (1).

The set up of the experiment is shown in the following:

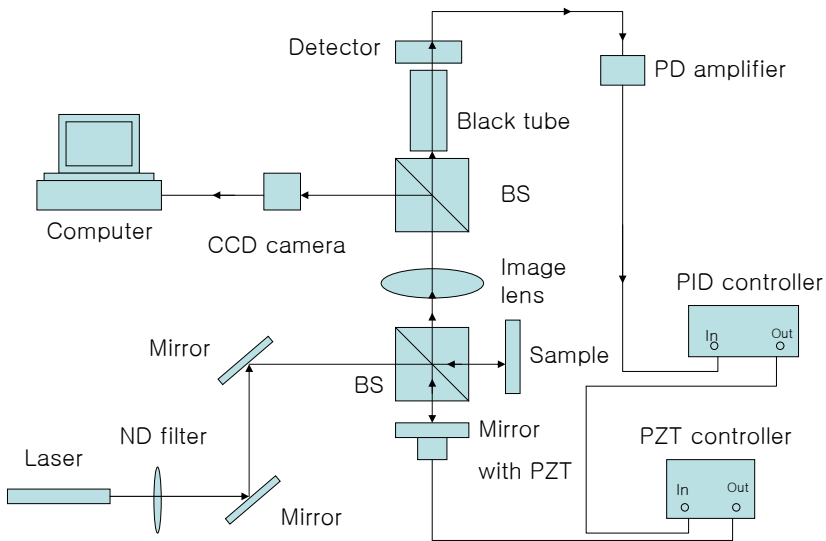


Fig.2.4: Set up of the experiment of surface measurement

2.3 The procedure of tuning the parameters of PID controller

In order to get the stabilization of the surface measurement system, we tuned the parameters of the PID controller carefully. The procedures for those are introduced in the following paragraph.

The procedure of adjusting the PID controller so as to get the stabilization is shown as the following:

1. Set up the Twyman–Green interferometer.
2. Connect the reference mirror and the PZT controller (PZT and sensor pins on the front panel).
3. Connect the photo diode and the input of the PID controller by the photo diode amplifier PAD-S.
4. Connect the output of the PID controller to the input of the PZT controller, and connect it to the channel 2 of the oscilloscope.
5. Connect the monitor output of the PID controller to the channel 1 of the oscilloscope.
6. Connect the CCD camera to the monitor.
7. Check all of the connections and power supplies, then turn on the laser system, the diode laser system DL100, the PZT servo controller, the oscilloscope and the monitor one by one.
8. Check the operation controls on the PID regulator.

Turn the gain precision potentiometer to position 3.

Turn on the Reg. ON/OFF switch so as to close the control loop of feedback.

Turn off the Ramp ON/OFF switch.

Turn the POS/NEG Switch to position POS so that the regulator stabilizes on a rising edge.

9. Wait about half an hour until the stabilization lamp on the front panel of the laser system changed to light. Adjust the monitor selector switch of the PID regulator on input position, observe the input signal on the screen of the oscilloscope, adjust the DC offset knob from zero clockwise, write down the minimum value and the maximum value, and calculate the mean value of them as the set point value. Then change the selector switch of the PID regulator on set point position, determine the voltage level to define the locking point.
10. Adjust the PAD-S gain in position 6, the stepless adjustment of the photo detector input amplification via potentiometer (10% to 100%) is in low position.
11. Adjust the output range trimpot in a proper position, this trimpot for adjusting the maximum output voltage at Output BNC-connector.
12. Increase the P trimpot from zero position clockwise by small driver until oscillation produced, then decrease the P value slightly, it is the optimal position which we need.

13. Increase the I trimpot from zero position clockwise by small driver until an oscillation produced, then decrease the I value slightly, it is the optimal position which we need.

14. Because we know the utmost right position, we adjust the D trimpot from maximum. Decrease the D trimpot counter clockwise and observe the input signal and output signal until we get the stabilization point. The input signal is near constant.

2.4 Discussion about the order of fringe stabilization:

We obtained a group of data by analyzing the fluctuations with respect to the time without the stabilization of the interferometer and with the stabilization of the interferometer.

1. without stabilization:

| | |
|--------------------------------|---------------------------|
| Standard Deviation (Sd) | 0.107 (V) |
| Standard Error of the mean(Se) | $1.576 \cdot 10^{-3}$ (V) |

Table.2.1: Statistical parameters under the condition without stabilization

2. with stabilization:

| | |
|--------------------------------|---------------------------|
| Standard Deviation (Sd) | 0.0147(V) |
| Standard Error of the mean(Se) | $1.999 \cdot 10^{-4}$ (V) |

Table.2.2: Statistical parameters under the condition with stabilization

3. Comparison of the stability between without stabilization and with

stabilization:

| | |
|--------------------------------|-----------------------------------|
| Standard Deviation (Sd) | $0.107/0.0147=7.3$ |
| Standard Error of the mean(Se) | $1.576*10^{-3}/1.999*10^{-4}=7.8$ |

Table.2.3: Comparison of statistical parameters between without stabilization and with stabilization

Above results illustrate that the ability of eliminating the drifts under stabilization by PID controller is better than the instance which is without stabilization about 7 times. The drifts with stabilization are merely 1/7 of that without stabilization.

The main parameters under the condition of experiment are shown below:

- (1) The temperature in the lab is 24°.
- (2) The peak to peak amplitude of fluctuation voltage of the error signal without stabilization is 648mV.
- (3) The difference between maximum and minimum amplitude of signal with stabilization is 160mV, however most of the amplitude was changed range less than 40mV.

2.5. Application of the PZT controller

Next, we can measure the wavelength of the laser source by the setup of the experiment.

The positions of actuator of the PZT controller are shown as the following:

| | input voltage | displacement of mirror |
|--------|---------------|------------------------|
| Group1 | 16.03V | 3.249 μ m |
| | 17.94V | 3.572 μ m |

Table.2.4: Records of experiment about input voltage and displacement of mirror (1)

From the minimum of the input signal, we get the value 16.03 V, displacement of the mirror from origin is 3.249 μ m at that time. From the maximum of the input signal, we get the value 17.94 V, displacement of the mirror from origin is 3.572 μ m at this point.

The variation range of the input voltage is 1.91V. The subtraction of two displacements is 0.323 μ m. We know that the wavelength of the laser beam travel from minimum to maximum in 1/2 period of fringe, and the optical difference is changed in $\lambda/2$. Travel from minimum to maximum positions also means the position grabbed by the photo diode was moved half fringe (center of bright band to center of dark band). Because the laser beam was reflected by the mirror, the optical path distance is two times of the displacement of the mirror moving. The OPD is 643nm (323nm*2). We can calculate the wavelength λ of He-Ne laser is 643 nm. It is known that wavelength λ of He-Ne laser is 632.8nm, the error is 643-632.8=10.2nm.

| | input voltage | displacement of mirror |
|--------|---------------|------------------------|
| Group2 | 17.83V | 3.573 μ m |
| | 20.02V | 3.888 μ m |

Table.2.5: Records of experiment about input voltage and displacement of mirror (2)

The variation range of the input voltage is 2.19V. The subtraction of two displacements is 0.315 μ m. According as the same analysis above, we can get the result of the second group of data. The OPD is 315nm*2=630nm. We can calculate the wavelength λ of He-Ne laser is 630 nm. It is known that the wavelength λ of He-Ne laser is 632.8nm, the error is 630-632.8=-2.8nm.

Obviously, the second group of result is better than the first one.

Without the photo diode preamplifier PDA-S, the amplitude of signal is too weak to be controlled by the PID regulator, the stabilization can not be completed. It is also the reason why we must use the photo diode amplifier PDA-S to complete the experiment.

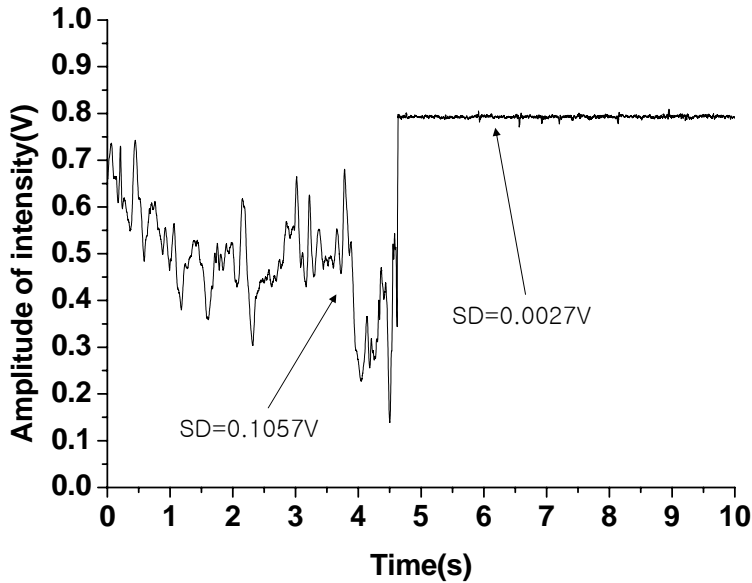


Fig.2.5: Comparison for intensity of PD between with stabilization and without stabilization

As shown in Fig.2.5, at about 4.5 s, the servo of stabilization system is turned on. The signal trends without (left) and with (right) stabilization is obvious. On the left, the signal fluctuated dramatically (fringes moving dramatically) due to the strong perturbations such as the wind flowing and the person passing by the table^[16]. On the right, after turning on the closed feedback loop of stabilization system, the changing of OPD is corrected effectively and the interferometer is stabilized successfully.

2.6 The results of the step height measurement with Fourier transform method and roughness amplitude parameters

By using the Fourier transform method, we obtained the calculated surface profile about the step height, the following figures showed the results.

In order to compare the figures with stabilization and without stabilization conveniently, we displayed two groups of figures on the left and right respectively.

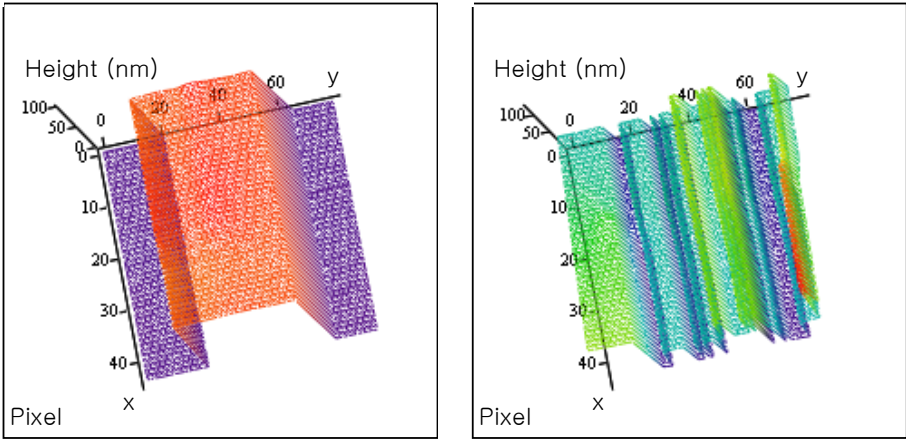


Fig.2.6: Comparison about the calculated surface profile of step height with (L) and without (R) stabilization

The step is 100 micrometers wide and 750 micrometers in length. Using equation $H(x) = (\lambda/4\pi) \cdot \phi(x)$ in matrix calculation, we found the step height to be (93.1 ± 1.2) nm and the real value of every pixel in horizontal direction is 2.04 μ m/pixel (100 μ m/49 pixels).

In fact, the calibrated step height certificated by VLSI standards incorporated is (93.2 ± 1.4) nm as is recorded in the certificate of calibration.

In the experiment, we measured the sample of step height totally five times. The measured values are 92.17 nm, 93.93 nm, 94.90 nm, 92.60 nm, 92.06 nm, under the stabilization of the interferometer, respectively. We calculated the mean value of them, and obtained the uncertainty by calculating the standard deviation of them. So the calculated result is 93.1 ± 1.2 nm.

Above we have discussed how to obtain the total value of recorded data which are derived from the experiment. In the following the paragraph, we will discuss how to calculate the roughness amplitude parameters.

There are many surface roughness parameters about surface profile measurement such as roughness average (Ra), root mean square roughness (Rq), maximum height of the profile (Rt), roughness height (Rz (iso)) etc. Ra, Rq, and Rz (iso) are primary parameters in them. We introduce them in the appendix(2).

The table of results of experiment is shown in the following.

| Roughness amplitude parameters | Calculated value | | | | |
|--------------------------------|------------------|--------|--------|--------|--------|
| | Group1 | Group2 | Group3 | Group4 | Group5 |
| Ra | 2.38nm | 1.93nm | 1.48nm | 3.23nm | 2.32nm |
| Rq | 2.91nm | 2.15nm | 1.87nm | 3.54nm | 2.69nm |
| Rz | 3.80nm | 1.86nm | 3.12nm | 1.82nm | 6.44nm |

Ra: center line average roughness

Rq: root-mean-square roughness

Rz : ISO, 10 points height parameter

Table.2.6: Five group of calculated roughness amplitude parameters

| Roughness amplitude parameters | Calculated value |
|--------------------------------------|------------------|
| Ra (center line average roughness) | 2.27 nm |
| Rq (root-mean-square roughness) | 2.63 nm |
| Rz (ISO, 10 points height parameter) | 3.41 nm |

Table.2.7: The results of calculated roughness amplitude parameters

The results which are obtained from the experiment are shown in above tables. The procedures and more details about the calculations of these parameters are displayed in the appendix (2).

2.7 Surface measurement by ACCURA system

In order to get another results to be compared, we used the Accura optical dimensional metrology machine to measure the step height once more. This surface profiler is compact Mirau type interferometer on the vibrationless optical breadboard.

The cross-section results of obtained surface profile are shown in the following:

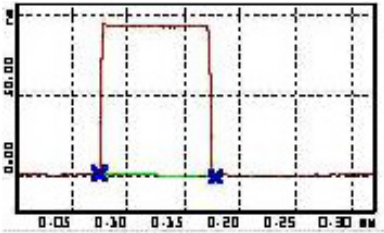


Fig.2.7: The result of measurement in 2D.

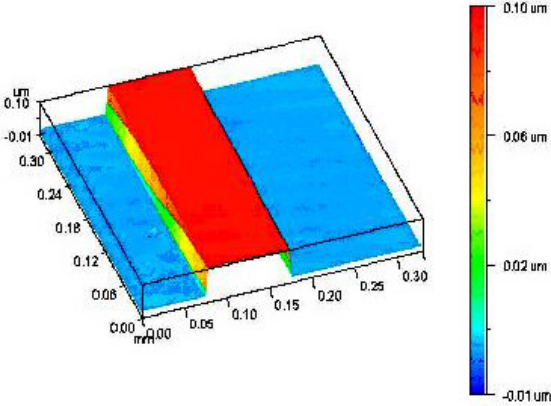


Fig.2.8: The result of measurement in 3D

The step height value measured by Accura2000 is 0.093 μm and the width of the step is 103.17 μm and height is 93.0 nm.

2.8 The comparison of the results between with stabilization and without stabilization, and comparison of results between by FFT method and by ACCURA 2000 system.

As above introductions, in the experiment, we developed a program for measuring the step height, at first, we measured it with stabilization, then measured it again without stabilization, compared the results in different conditions. Next we used the Accura 2000B system to measure the step height by Accura optical dimensional metrology machine and got the precise value of the step height. Comparing the two values between using the Twyman-Green interferometer with stabilization and Accura 2000B system we discussed about the results. We have compared the results between with stabilization and without stabilization. It is obvious that the result with stabilization is better than the result without stabilization. Only through analyzing the image which is captured by the CCD camera with optical system of stabilization, we can measure the step height successfully. Without stabilization, the perturbations such as air flowing, thermal drift, etc. will change the OPD of the reference or the object, and the phase map which we need will be distorted seriously, it is difficult to get surface measurement.

We compared the results between using the Twyman- Green interferometer and using the Accura optical dimensional metrology

machine. The results displayed that the latter one is better. We analyzed it is because that the components inside the machine are more compact and the vibrations inside the machine are less than on the table which has no covers to prevent the perturbations from air. So we can get the clearest phase map inside the machine, i.e. we should improve our conditions of experiment so as to get better results than before.

| | |
|---|-------------------|
| Calculated height value and uncertainty | 93.1 ± 1.2 nm |
| Calibrated height value and uncertainty measured by VLSI standards incorporated | 93.2 ± 1.4 nm |
| Height value measured by commercial ACCURA 2000 system | 93.0 nm |

Table.2.8: The comparison of results between ours and commercial ones of the experiment

The comparison of results by different ways is shown in Table.2.15, it should be demonstrated that there is no uncertainty shown by the ACCURA2000 system. It is a defect in this system and it should be improved in the future.

II. The frequency stabilization of diode laser by PID controller.

3. The frequency stabilization of diode laser by PID controller.

3.1 Introduction and principles

3.1.1: Introduction

There are several ways such as a Hänsh-Couillaud, Pound-Drever-Hall (PDH) locking, etc. to stabilize the cavity^[17]. Tilt locking method among these techniques were developed to measure gravitational wave with the interferometer. We employed this method to measure the hyperfine manifold of ^{85}Rb and stabilize the diode laser frequency. The principles if this tilt locking were described well in the previous works^[3]. That used the interference between the fundamental Gaussian mode of the cavity and non-resonant higher order spatial mode. When this carrier field drifts slightly away from the cavity resonance, an error signal can be obtained. We use this signal to stabilize the laser signal.

We have introduced the application PID controller in the close feedback loop system about surface measurement in above chapter. In fact, the PID 100 regulator is especially designed for diode laser system DL 100. Recently, frequency locking techniques are more and more important in the field about application of diode laser such as laser frequency stabilization, and gravitational wave detection, etc. In general, the frequency locking techniques require the generation of an error signal

which is proportional to the difference between the laser frequency and the cavity resonance. Refer to the frequency stabilization of diode laser, we should know the technology named tilt locking.

In traditional method, we used the PID 100 to laser frequency stabilization to the edge of an atomic absorption resonant line, as well as to the edge of a more narrow, according to spectral width, “Doppler-free” saturated lines of ^{85}Rb . In our case, we utilized a novel Sagnac interferometer to create an error signal from saturated-absorption spectroscopy for Rubidium D_2 lines and we used the PID controller for laser stabilization to the edge of the error signal generated by the quadrant photo diode in the set up of the Sagnac interferometer.^[4]

3.1.2: Basic knowledge about characteristics of Rubidium

Rubidium belongs to the group of alkali metals. The ground electron configuration of rubidium is $1s^2, 2s^2, 2p^6, 3s^2, 3p^6, 3d^{10}, 4s^2, 4p^6, 5s^1$. Rubidium in nature is a mixture of the two isotopes ^{85}Rb and ^{87}Rb . The isotopes have different nuclear and abundance^[18].

| Isotopes | Nuclear spin I | Relative abundance |
|------------------|----------------|--------------------|
| ^{85}Rb | 5/2 | 0.722 |
| ^{87}Rb | 3/2 | 0.278 |

Table.3.1: some features of Rubidium

As the theory of atomic fine and hyperfine structure, the atomic fine structure originates from an interaction of atomic magnetic fields and magnetic moments of electron spin and orbit. Fine structure interaction splits up the Rubidium P level into $5P_{1/2}$ and $5P_{3/2}$. Fig.3.1 shows energy level diagram of ^{85}Rb and ^{87}Rb , the hyperfine structure of the $5S_{1/2}$, $5P_{1/2}$ and $5P_{3/2}$ level value in MHz.

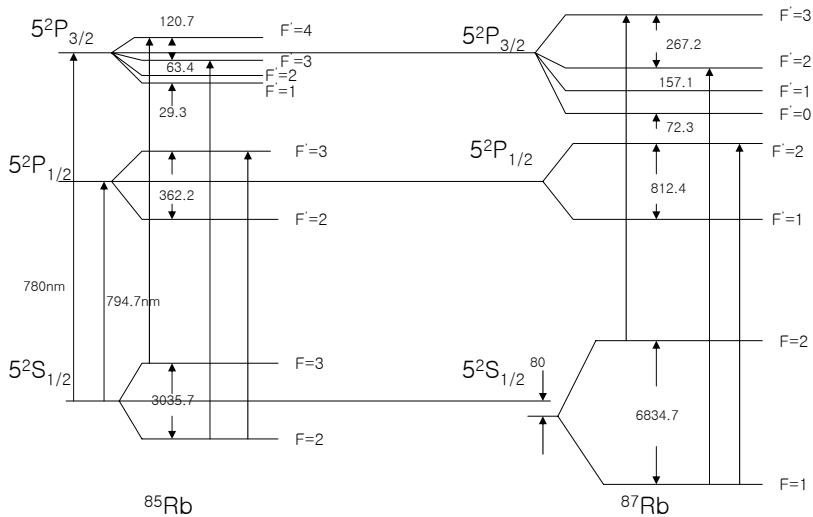


Fig.3.1 Energy level diagram of ^{85}Rb and ^{87}Rb showing the hyperfine structure of the $5S_{1/2}$, $5P_{1/2}$ and $5P_{3/2}$ level value in MHz

3.2 Experimental setup and analysis for the results of experiment

3.2.1 Tilt locking

Tilt locking is a novel technology for laser frequency control. It has been used in many fields especially in laser frequency stabilization. There are several methods for obtaining an error signal such as fringe side locking, transmission locking, Hansch Couillaud locking and Pound-Drever-Hall locking^[17]. Comparing above methods, the tilt locking technique has many advantages^[4]. For example, the optical-electronic components of the tilt locking system are not expensive. TEM stands for spatial transverse electro-magnetic mode. These modes can be approximated by the Hermite-Gauss functions. The electric fields of the first two Hermite-Gauss modes, the TEM₀₀ and TEM₁₀ modes are displayed respectively below ^[3]:

$$u_0(x) = \left(\frac{2}{\pi}\right)^{\frac{1}{4}} \left(\frac{1}{w}\right)^{\frac{1}{2}} e^{-\left(\frac{x^2}{w^2}\right)} \quad (31)$$

$$u_1(x) = \left(\frac{2}{\pi}\right)^{\frac{1}{4}} \left(\frac{1}{w}\right)^{\frac{3}{2}} 2xe^{-\left(\frac{x^2}{w^2}\right)} \quad (32)$$

Tilt locking relies on the fundamental TEM_{00} mode and the TEM_{10} mode interference to obtain an error signal.

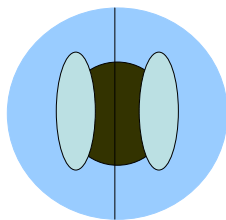


Fig.3.2: Intensity distribution of TEM_{00} (dark circle) and TEM_{10} (light ellipses) on the split photodiode

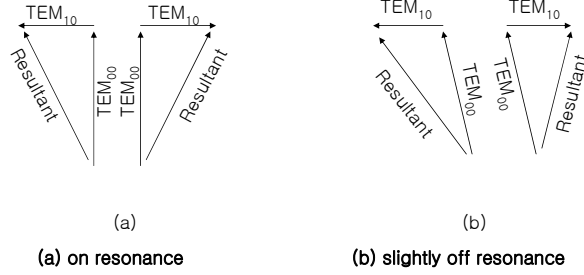


Fig.3.3: Vector summation of electric fields on each photo diode half with TEM₀₀

As shown in Fig.3.2, a two element, split photodiode is used to detect the beam reflected from the cavity. By subtracting the outputs of the two photodiode halves an error signal is obtained. The interference measured by this split detection is given by the following equation^[17]:

$$I = \left| \int_{-\infty}^{\infty} \int_{-\infty}^0 u_{00}^*(x, y) u_{10}(x, y) dx dy \right| - \left| \int_{-\infty}^{\infty} \int_0^{\infty} u_{00}^*(x, y) u_{10}(x, y) dx dy \right| \quad (33)$$

For tilt locking, the input beam is aligned and to give only TEM₀₀ mode and a TEM₁₀ mode with a relative phase of $\pm 90^\circ$ at the plane of photo detector. When TEM₀₀ mode is exactly resonant with the cavity and the TEM₁₀ is non-resonant, the interference is shown in Fig.3.3

(a), and the phase shift is not added by the cavity. On left half, the TEM_{10} adds to the TEM_{00} mode with 90° phase, and on right half, the TEM_{10} adds with -90° phase. As the theory of summation of two vectors, the magnitudes and directions of the vector of resultant are shown in the Fig.3.3. What we cared here was the magnitudes of the two resultant vectors, because the power of each half is proportional to the square of the resultant vector. It is obvious to know that the powers of the two halves are same value. The error signal is zero.^[17]

When the TEM_{00} mode is slightly away from resonance due to the misaligned by the cavity, the TEM_{00} mode get an equal phase shift in both photodiode halves and in the same time the non-resonant TEM_{10} mode remains unchanged as shown in Fig.3.3 (b). We found that the resultant vectors of two halves are not only in different directions, but also in different magnitudes. The magnitudes of two resultant vectors of two halves are different so that it led to the electronically subtracted photo-current by the electronic board give the error signal to the output^[17].

3.3 The set up of the experiment

The experiment setup is shown in the Fig.3.7. The DL100 laser beam^[19] of TUI company is splitted into two beams. One is directed into Sagnac interferometer and the other into Fabry-Perot interferometer for the transmission curves for the frequency interval

references. Rubidium cell is positioned inside Sagnac interferometer and the power of one beam is strong as a pump beam and the other is weak as a probe beam. When the probe beam is scanned in the hyperfine manifolds [$5^2S_{1/2} F3 \rightarrow F'=2, 3, 4, 5^2P_{3/2} \text{ } ^{85}\text{Rb}$], the phase shift due to the change of the refractive index of the atoms makes the constructive interference between the TEM_{00} and TEM_{01} mode from the cavity modes, so that an error signal can be obtained by using this error signal. This error signal is forwarded into the quadrant photodiode and amplified and passed to a servo loop for the stabilization of the laser. For the feedback loop we used is a general proportional integral differential regulator circuit.

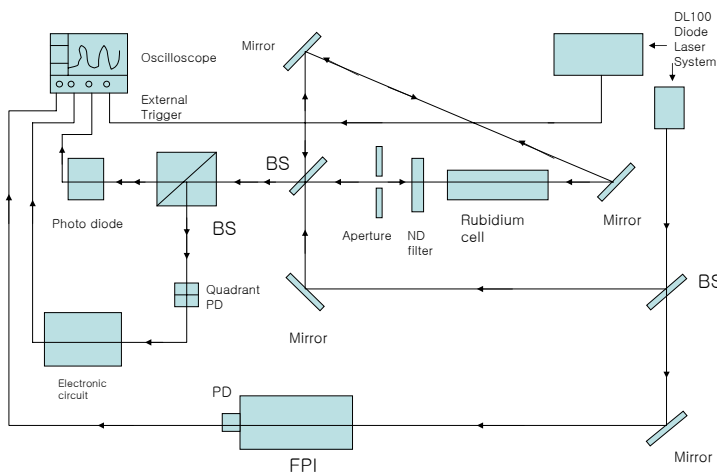


Fig.3.4: The optical block diagram about laser frequency stabilization using the regulator PID 100^[19].

It should be demonstrated that the setting of the stabilization point-set point. We have mentioned that it is very important to get the fine adjustment about the stabilization level set point during the closed feedback loop. The set point can be adjusted according to the amplitude of the photo diode amplifier or the intensity of the photo diode. In the experiment, the set point of PID 100 is optimized by the trimpot (9) on the front panel. On the PID 100 front panel, there is a monitor selector switch, we made its position into “SET” and watch the set point level on the oscilloscope, compared the input signal simultaneously to determine the optimum stabilization level. In most time, the mean value of the maximum value and the minimum value of the input signal is near the best set point level. As the theory, we can obtain the side-of-fringe stabilization due to the steepest slope of the fringe-signal, so the procedure of adjusting the set point level is the same as to look for the steepest slope of the fringe-signal so as to obtain the firm locking to the edge of signal. In the procedure of tuning the PID parameters, we observe the error signal with the monitor output. When the system which is controlled is locked, the error signal on the oscilloscope should be constant. ^[15]

3.4 Results of the experiment and Discussion

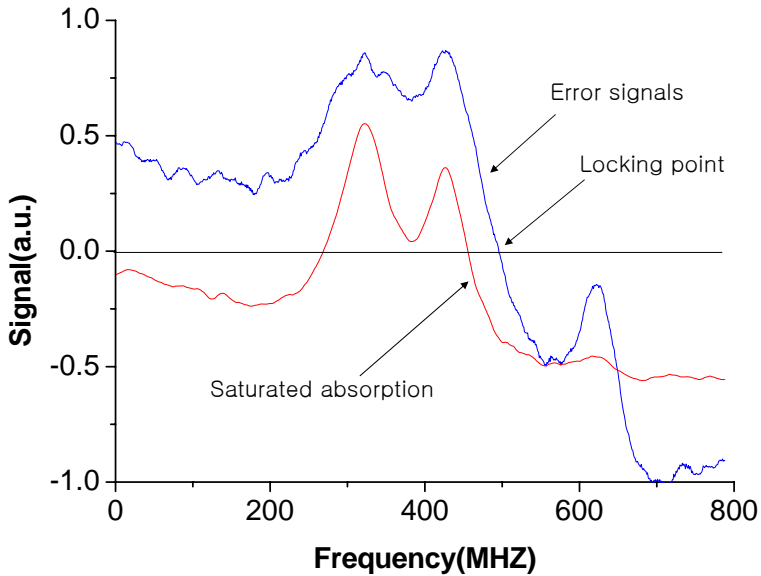


Fig.3.5 Saturated absorption and error signals generated by the interferometer tilt-locking system, measured $^{85}\text{Rb } 5^2 S_{1/2}, F_3 - F'4 \rightarrow 5^2 P_{3/2}$

As shown in Fig.3.5, $^{85}\text{Rb } 5^2 S_{1/2}, F_3 - F'4 \rightarrow 5^2 P_{3/2}$ saturated absorption and error signals generated by the interferometer tilt-locking system are measured. The atomic transitions are shown obviously in two lines and the selection of the locking point is also pointed out. It is necessary to select the steepest line of error signal for being locked.

Before we stabilized the line of the error signal, the spectral range of scanning of the laser diode should be optimized. If there are many lines

being tight together, it is very important to single out one line to be locked without perturbed by adjacent lines. We should reduce the scan width to cover only one line which we wanted to stabilize before tuning the PID parameters of the close loop^[19]. There are two methods about reducing the scan width, one is to increase the modulation frequency. Another one is to decrease the modulation amplitude. In general, the latter method is more used.

The input signal come from photo diode amplifier enters the PID 100 controller by the sub-connector on the front panel. The PID 100 in combination with the scan control SC100 has been demonstrated before. The following words described the course of obtaining stabilization point:

1. Initial setting: the overall Gain Precision Potentiometer should be tuned to position 3 or 4 and all of P, I, D trimpots should be to their utmost left stop. The scan ramp out of the SC100 as the trigger source enters the external channel of the oscilloscope.
2. Observing the input signal on the screen of oscilloscope, obtaining the optimal signal by tuning the switchable gain and the level of voltage offset of photo diode amplifier. Set up the oscilloscope to be DC-coupled and adjust the voltage offset in a proper level.
3. Switch the monitor selector switch to SET position, the line of signal which we want to lock should be selected and tuning the set point trimpot to obtain the optimal set point level. The

frequency of intersection of the Set Point line and the input signal will be locked by PID controller. As is explained before, it is very important to select the line which is steepest slope. It is the key factor to get the frequency stabilization successfully.

4. Now the Regulator PID 100 should be switched on, start adjusting the P, I, D trimpots so as to get the frequency stabilization. At first, increase the I (integral) trimpot of the regulator until a regulator output signal can be observing by switch the monitor switch in REG position. Go on increasing the P parameter until an oscillation produced by a very high value, decrease the P parameter slightly until without oscillation, go on decreasing about 2-3 turns. Increase the values of trimpots P and D until an oscillation is generated again due to high value. Decrease P and D levels until no oscillation occurs anymore. Up to here, the optimal adjustment of P, I, and D is obtained^[19]

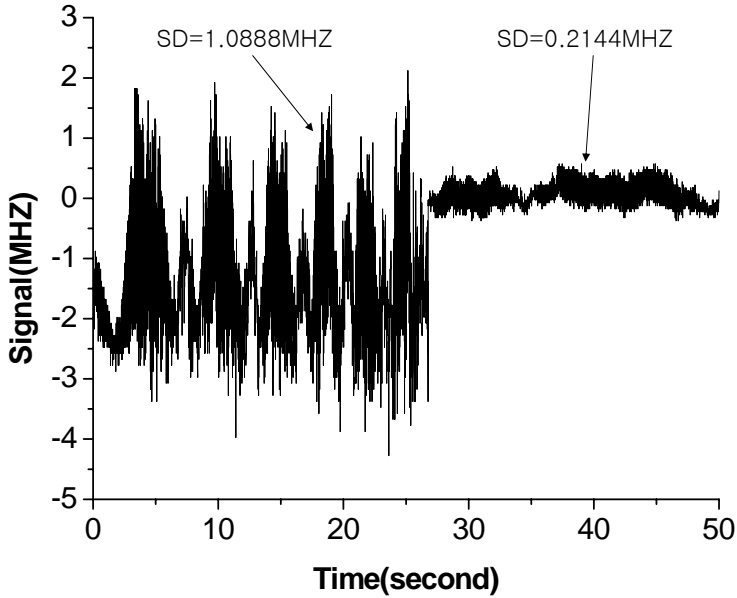


Fig.3.6: Free running and PID locked laser frequency fluctuations from 27s

We checked the stabilization of the laser as shown in Fig.3.6. Servo lock was turned on at around 27 s of the free running of the laser. The result shows that the laser frequency is stabilized up to sub-megahertz level as shown in Fig.3.6. Also we will discuss the applications such as surface profile measurement, gravitational wave measurement, etc. by using that stabilized Sagnac interferometer.

As the conclusion, tilt locking technology has significant advantages over previously methods. We have set up the Sagnac interferometer and used the PID controller of the DL 100 system to realize the frequency

stabilizing of a diode laser to an atomic transition. Finally, we offered the firm sub-megahertz frequency stabilization for the diode laser. The result is shown on Fig.3.6.

Acknowledgements

The procedure of experiment and analysis of results is not easy for me, it contains the wisdoms and labors of my advisor Professor Kim, Jin-Tae, Ph.D., and Professor Kim, Hyun Su, Ph.D., Professor Park, Jong Rak, Ph.D., Dr. Kapitanov Ph.D.(Russia). Without their help and guidance, I can not accomplish the experiment and the thesis. I must thank them for their important directions and helps. Especially, my advisor Professor Kim, Jin-Tae, Ph.D. gave me great encourage so that I can complete my experiment and thesis. In past two years, my parents, my wife and my son always gave me much good advice so that I could overcome all of difficulties and accomplish my tasks, I should also thank them heartily.

References

1. Mitsuo Takeda, Hideki Ina* and Seiji Kobayashi, "Fourier transform method of fringe-pattern analysis for computer-based topography and interferometry," J. Opt. Soc. Am. /Vol. 72, No.1 / 1982, pp.1~4.
2. Thomas Kreis, "Digital holographic interference-phase measurement using the Fourier-transform method" Vol. 3, No.6 / 1986/J.Opt.Soc.Am. A, pp.1~8.
3. Daniel Anthony Ahaddock, "Advanced interferometry for gravitational wave detection" a thesis submitted for the degree of PhD at the Australian National University submitted, 2000, pp.20~21, 105, 110~112.
4. N. P. Robins, B. J. J. Slagmolen, D. A. Shaddock, J. D. Close, M. B. Gray, "Interferometric modulation-free laser stabilization," 1905 Vol.27, No.21/OPTICS LETTERS (2002), pp.1~3.
5. Munther, A. Gdeisat, David R. Rurton, and Michael J. Lalor, "Fringe pattern demodulation with a two-frame digital phase-locked loop algorithm" 10 September 2002/Vol.41, No.26/ Applied Optics, pp.1.
6. Kim, Cheol Jung, "Development of laser materials processing and laser metrology techniques" 7, 1994, pp.238~269.
7. Canan Karaalioglu, Yani Skarlatos, "Fourier transform method for measurement of thin film thickness by speckle interferometry," 1694 Opt.Eng.42 (6)1694-1698 (2003), pp.1~2.

8. T. R. Judge, "The automatic analysis of interferometric data" Optical Engineering Laboratory 1996, pp.1, 5~7.
9. William W. Macy, Jr, "Two-dimensional fringe-pattern analysis" 3898 APPLIED OPTICS/Vol.22,No.23/1 1983, pp.1~4.
10. "Ultraprecision surface measurement by phase-measuring interferometry (I)", pp.48~56, 59~74, 107.
11. Kie B. Nahm, "Fourier transform method of surface topography and interferometry" the journal of optical society of Korea Volume 3, Number 1, 1992, pp. 1~5.
12. Liu Zhen, Hyun Su Kim, Jong Rak Park, Ho-Jae Lee, Jin-Tae Kim, "Technology of Surface Profile Measurement by Using Fast Fourier Transform Method," Graduate School, Dept. of Applied Optics, Chosun Univ, Micromaching Team, Kitech, Dept of Photonic Engineering, Chosun University, pp.1~2.
13. "Stabilock II active fringe stabilizer user manual" Odnher Hoolographics, pp.8~9.
14. "Process dynamics and control" Seborg, D. E., Edgar, T. F., and Mellichamp, D. A. Wiley, New York, 1989, pp.1~2.
15. "What is PID-tutorial overview" 1999-2005 Expertune, Inc. Lake country research center 1020 James drive, Suite A Hartland WI 53029-8305 USA. pp. 1~2.
16. Jin-Tae Kim, "Stabilization of the Constructed Polarization Phase Shifting Interferometer Module," Department of Photonic Engineering, Chosun University, pp.1~2.

17. D. A. Shaddock, M. B. Gray, and D. E. McClelland, "Frequency locking a laser to an optical cavity by use of spatial mode interference." August 25, 1999, pp.1~2.
18. Jan Max Walter Kruger, Andrew Wilson, "A novel technique for frequency stabilizing laser diodes" University of Otago 1998, pp.5, 9~10.
19. "DL100 diode laser system manual" Toptica photonics, Germany, Part VIII Scan Control SC 100, pp.3~13, Part X PID Regulator PID 100, pp.3~24.

Appendix

(1) The specifications of the components for the experiment

1. Step height standard

The step height is the sample which we should measure in the experiment. In the model number, Q identifies the substrate as quartz, C means chrome coated.

| | |
|---------------|---------------------------------------|
| Manufacturer | VLSI standards incorporated |
| Model Number | SHS-880 QC |
| Serial number | 5904-70-18 |
| Step material | Step etched in quartz (Chrome-coated) |

Table.4.1: Specifications of step height standard

2. Laser source

The specification of laser source is shown in the following table.

| | |
|--|-------------------------------------|
| Manufacturer: | Melles Griot Inc |
| Laser | He-Ne (632.8 nm) |
| Model | 05STP 903 |
| Beam Diameter | 0.50mm |
| Power | 1.0mw |
| Beam Divergence | 1.60 mrad |
| Power Stabilized mode (1min./1hr/8hrs) | $\pm 0.1\% / \pm 0.2\% / \pm 0.2\%$ |

Table.4.2: Specifications of laser source

3. Piezo controller

The Piezo controller is used in the experiment for driving the reference mirror which is adhered with Piezoelectric.

| | |
|----------------------|-------------|
| Peak power | 200w |
| Output voltage range | -20 to 120V |

(a): Specifications of LVPZT amplifier module

| | |
|----------------|------------------|
| Channels | 1 (E-509.x1) |
| Rear connector | 32-pin connector |

(b) Specifications of Sensor & Position servo-control modules for PZTs

| | |
|----------------------|---|
| Function | 20-bit D/A converter interface/module, IEEE 488/rs-232 |
| Channels | 3 |
| Output voltage range | -1 to 11 V |
| Stability | better than 0.2 mV |
| Linearity | 0.01% |

(c) Specifications of computer interface & display module

Table.4.3: Specifications of PIEZO Controller

4. Photo Diode Amplifier with switchable gain

The photo diode amplifier is used in the experiment for pre-amplifying the voltage which is fed from the silicon photo diode.

| | |
|--|--|
| Bandwidth | 20 to 30 KHz |
| Current amplification | switch position (0---7) VS gain (1×10^5 V/A--- 2×10^7 V/A) |
| Adjustment of the input gain | 10% to 100% |
| Cut-off frequencies of the high pass filters | 10 HZ and 300 HZ |
| Supply voltage | + 12V (via included stabilized power supply unit) |

Table.4.4: Specifications of photo Diode Amplifier with switchable gain

5. Photo detectors

The silicon photo detector is used in the experiment for detecting and scaling the signal of fringes moving.

| | |
|-------------------|--------------------------------------|
| Part number | DET210 |
| Spectral response | from 200 nm to 1100 nm |
| Peak wavelength | $730 \text{ nm} \pm 50 \text{ nm}$ |
| Peak response | 0.45A/W |
| Rise/Fall time | 1 ns |
| Active area | $\phi 1 \text{mm} (0.8 \text{mm}^2)$ |
| Linearity | 1mW |

Table.4.5: Specifications of photo detectors

6. The Oscilloscope

The oscilloscope is used in the experiment for monitoring the various signals derived from PID controller and the input signal which

come from the PDA-S.

| | |
|---------------------|------------------------------|
| Model | Tektronix TDS 3052B |
| Bandwidth | 500 MHz, 300 MHz and 100 MHz |
| Sample Rates | up to 5 GS/s |
| Vertical Resolution | 9-Bit |

Table.4.6: Specifications of the Oscilloscope

7. The PID controller^[19]

The PID controller is used in the experiment for generating control signals and sending the signals to the PZT controller.

Model: the regulator PID 100 for DL100 diode laser system



Fig. 4.1: The front panel of PID 100

Accessible Parameters:

- P, I, D –can be adjusted individually by precision trimmer
- Set Point for the control loop, e.g. stabilization to side-of-fringe of a line
- Useful display of the control lock status with 3 LEDs (search, unlock, reset)
- Ramp/Modulation ON/OFF switch and Regulation ON/OFF switch
- Inversion of the Control Output with switch POS/NEG
- Red Relock-LED
- External modulation input or internal synchronisation with Scan Control SC 100
- Controller ON/OFF switch ^[17]

8. CCD camera

The CCD camera is used in the experiment for capturing the images which will be analyzed for FFT method.

| | |
|----------------------------------|---|
| Model | SONY XC-HR50 |
| Speed of reading images | 60 fps |
| Sensor size | 5.84x4.94 mm (H/V) |
| Horizontal resolution | 500 TV/lines |
| Number of effective pixels | 659x494 (H/V) |
| Shutter speed | External trigger shutter:1/4 to 1/100000s |
| Scan lines | 525-line |
| Output signal frequency | 59.94 Hz |
| CCD vertical driving frequency | 31.468 kHz±1% |
| CCD horizontal driving frequency | 24.5454 MHz |

Table.4.7: Specification of CCD camera

Calculations of camera resolution about the CCD camera:

Camera resolution (lines pair/mm):

$$=TVL \text{ (horiz)} \times 1.33/[2 \times (\text{sensor size})]$$

$$=500 \times 1.33/(2 \times 5.84 \text{mm})$$

$$=57.0 \text{ lines pair/mm}$$

(2) The calculations about roughness amplitude parameters

I: Ra - Average Roughness

The average roughness is the area between the roughness profile and its mean line, or the integral of the absolute value of the roughness profile height over the evaluation length:

$$R_a = \frac{1}{L} \int_0^L |r(x)| dx \quad (1)$$

When evaluated from digital data, the integral is normally approximated by a trapezoidal rule:

$$R_a = \frac{1}{N} \sum_{n=1}^N |r_n| \quad (2)$$

II: Rq - Root-Mean-Square Roughness

The root-mean-square (rms) average roughness of a surface is calculated from another integral of the roughness profile:

$$R_q = \sqrt{\frac{1}{L} \int_0^L r^2(x) dx} \quad (3)$$

The digital equivalent normally used is:

$$R_q = \sqrt{\frac{1}{N} \sum_{n=1}^N r_n^2} \quad (4)$$

III: Rz (ISO)

Rz (ISO) is the sum of the height of the highest peak subtracting the lowest valley depth within a sampling length. The 10 points height parameter Rz (ISO):

$$R_z = \frac{1}{5} \left(\sum_{i=1}^5 y_{p_i} - \sum_{i=1}^5 y_{v_i} \right) \quad (5)$$

After obtaining five groups of roughness amplitude parameters, we calculate the total center line average roughness, total root-mean-square roughness and total 10 points height parameter as the following equations:

$$R_a = \frac{\sum_{i=1}^5 (N_i \cdot R_{a_i})}{\sum_{i=1}^5 N_i} \quad (6)$$

Where N_i is the number of samples of every group, R_{a_i} is the value of center line average roughness of that group, and $i=1, 2, 3, 4, 5$.

Took the data into the equation, we obtained the total result of center

line average roughness is 2.27nm.

$$R_q = \frac{\sum_{i=1}^5 (N_i \cdot R_{qi})}{\sum_{i=1}^5 N_i} \quad (7)$$

Where N_i is the number of samples of every group, R_{qi} is the value of root-mean-square roughness of that group, and $i=1, 2, 3, 4, 5$.

Took the data into the equation, we obtained the total result of root-mean-square roughness is 2.63nm.

$$R_z = \frac{\sum_{i=1}^5 (N_i \cdot R_{zi})}{\sum_{i=1}^5 N_i} \quad (8)$$

Where N_i is the number of samples of every group, R_{zi} is the value of 10 points height parameter of that group, and $i=1, 2, 3, 4, 5$.

Took the data into the equation, we obtained the total result of 10 points height parameter is 3.41nm.

(3) About External Cavity Diode Laser and DL100 system^[19]

For DL100 system, free-running laser have a line width of about 100 MHz. Their emission frequency can be fine-tuned by adjusting current and temperature. The light emitted from the front facet of the laser diode is collimated by a multi-element lens with a very short length and then strikes a reflection grating. The grating is adjusted in the ‘‘Littrow’’ set-up.

The Littrow angle θ is determined by the equation:

$$\sin \theta = m\lambda / 2d$$

Where m is the diffraction order, λ is the wavelength of the incident light, d is the line spacing of the grating. In our case, $m=1$. The grating groove density widely used is 1800 lines/mm, the grating constant of $d=556\text{nm}$. At 780 nm, this leads to a refraction angle $2\theta=89.18^\circ$ for an output beam. [17]

It should be paid attention to that the grating feedback tuning range in the ECDL configuration is much larger than the temperature tuning range [18].

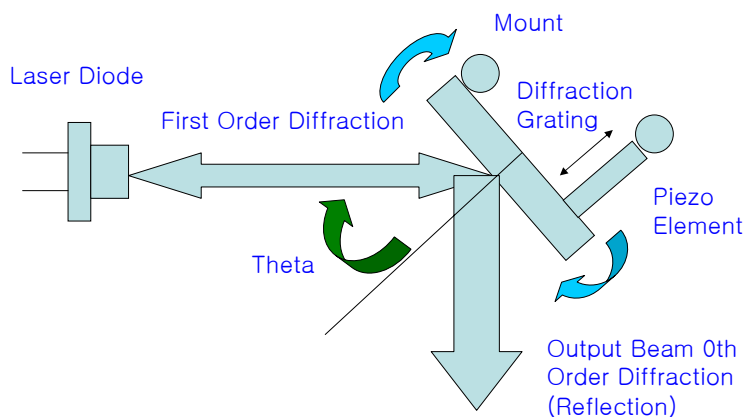


Fig.4.2: Diode/Grating in Littrow configuration